A Modular and Multimodal Generative AI Framework for Urban Building Energy Data: Generating Synthetic Homes

Jackson Eshbaugh[a,*], Chetan Tiwari[b,c], Jorge Silveyra[a]

[a]*Department of Computer Science, Lafayette College, 730 High Street, Easton, Pennsylvania, 18042, United States of America*
[b]*Departments of Geosciences & Computer Science, Georgia State University, 38 Peachtree Center Ave. SE, Suite 730, Atlanta, Georgia, 30303, United States of America*
[c]*Center for Disaster Informatics & Computational Epidemiology, Georgia State University, 38 Peachtree Center Ave. SE, Suite 730, Atlanta, Georgia, 30303, United States of America*

Abstract

Computational models have emerged as powerful tools for energy modeling research, touting scalability and quantitative results. However, these models require a plethora of data, some of which is inaccessible, expensive, or raises privacy concerns. We introduce a modular multimodal framework to produce this data from publicly accessible residential information and images using generative artificial intelligence (AI). Additionally, we provide a pipeline demonstrating this framework, and we evaluate its generative AI components. Our experiments show that our framework's use of AI avoids common issues with generative models. Our framework produces realistic, labeled data. By reducing dependence on costly or restricted data sources, we pave a path towards more accessible and reproducible research.

Keywords: Building Energy Models (BEM), Urban Building Energy Modeling (UBEM), Energy Policy, Synthetic Data, Generative AI

*Corresponding author.
Email addresses: eshbaugj@lafayette.edu (Jackson Eshbaugh), ctiwari@gsu.edu (Chetan Tiwari), silveyrj@lafayette.edu (Jorge Silveyra)

1. Introduction

Consumption of electricity in the United States rose approximately 57% from 1980 to 2009 [1] and seasonal electricity use per person has nearly doubled from 1973 to 2025 [2]. Rising energy consumption exerts increasing pressure on infrastructure capacity, operational costs, and greenhouse gas emissions, as well as costs for end-users. Accurate modeling and policy tools are therefore essential for effective planning, aiding by preventing infrastructure strain, optimizing energy costs, minimizing or mitigating climate impacts, assessing policy effectiveness, and guiding decision-making in urban centers [3, 4, 5, 6].

Computational approaches to monitor energy usage and model urban centers, buildings, and other structures require large amounts of data, such as type and quality of materials, floor plans, and weather patterns to produce scalable and quantitative results [7]. Moreover, several issues arise when attempting to collect such information, including high prices, limited availability, and privacy concerns. Consequently, these issues create barriers to accessing data, hindering the development of accurate models and scaling them to larger populations or geographic areas. The inaccessibility of this data has led researchers to generate synthetic data through a variety of methods. We propose a generative AI based approach to generate low-cost synthetic data that can used to develop, validate, and improve existing computational models for energy demand modeling. The proposed method enables the generation of large volumes of data for use in any geographic region where basic descriptive data on housing structures is publicly available.

Current data generation efforts span a wide range of approaches, from optimizing building construction processes to the creation of digital twins. Notably, Wan *et al.* [8] built a generative model that improves the efficiency of energy consumption by determining the optimal layout of floor plans. Elnabawi *et al.* [9] enhanced their building energy models using highly detailed microclimate models that considered features such as shadow generation and seasons to generate weather data. Lee *et al.* [10] train a neural network that predicts building energy consumption, aiming to create a more robust model with limited real-world measurements. The network was trained with data synthesized using electricity, temperature, and humidity, among others, encoded into receiver operating characteristic (ROC) plots which visually encode the separation between classes and are commonly used to assess model discrimination [11, 12].

Other researchers focus on creating and applying digital twins: virtual,

dynamic, and data-driven digital replicas of real-world urban environments. Stinner *et al.* [13] generate digital twins of building energy systems from piping and instrumentation diagrams using convolutional networks and other algorithms. Agostinelli *et al.* [14] create digital twins of energy efficient buildings in residential areas from Building Information Modeling (BIM), Internet of Things (IoT), Geographical Information Systems (GIS), and AI components, with machine learning serving as the central component of the model. Francisco *et al.* [15] take a different approach by generating digital twins of daily, time-segmented energy benchmarks solely from smart meter data streams. Finally, Belik and Rubanenko [16] present a hybrid digital twin framework for renewable energy sources (RES) that integrates real-time data, 3D modeling, and sensitivity analysis to improve forecasting and operational efficiency, particularly in grid systems with high RES penetration.

While prior work has focused on traditional simulation tools or sensor data to construct digital twins, Xu *et al.* [17] encourage the use of generative AI models, like GPT, because they present new opportunities in urban data generation. For instance, Dodge *et al.* [18] employ convolutional neural networks (CNNs) to parse floor plan images, generating structured representations using wall segmentation, object recognition, and optical character recognition. Relatedly, Zhang *et al.* [19] implement a pipeline that generates EnergyPlus IDF files from initial building geometry and textual building descriptions. Moreover, Xiao and Xu [20] propose a multi-agent LLM framework that processes unstructured building data and sensor logs to support automated energy optimization in smart grid contexts. Additionally, in closely related fields, generative AI has been successfully employed to perform a variety of tasks, such as predictive analysis of traffic congestion [21], real-time decision-making in urban air mobility [22], and stochastic solar irradiance forecasting for building facades [23].

Liu *et al.* [24] present a wide-ranging review on the integration of generative AI into building energy workflows, highlighting both opportunities and challenges. These include concerns such as dataset preparation, hallucinations, and a lack of domain-specific expertise. However, the impact of such challenges varies depending on the pipeline design. Because our framework combines pretrained LLMs with simulation tools for quantitative evaluation, we avoid the need for fine-tuning or physics-aware generation, thereby reducing the impact of these concerns. We evaluate our framework's LLM components to reduce hallucinations. Additionally, Liu emphasizes the importance of multimodal integration—where multiple data modalities (such

as image, text, and tabular data) are used by a process or model. Producing high-quality structured urban data suitable for tasks such as modeling and simulation requires combining multiple complimentary processes into a single workflow [25, 26, 27]. We adopt these principles in the design of our general framework.

In the following sections, we provide an in depth view of our framework (Section 2). Then, we test our pipeline's generative components (Section 3), ensuring the images are being processed correctly and the labels produced by the labeler are reflective of the inputs. Finally we conclude and highlight future directions from this work (Section 4).

2. Methodology

We propose a novel framework that combines multimodal real-world data with data generated using LLMs. We leverage open-access county data and generative AI to construct synthetic homes that mirror real-world counterparts and inspection notes corresponding to each. We then label this generated data using generative AI and a formula that ranks simulation results based on worst-case and best-case values. We test the ML components of our framework, extending beyond procedural evaluations. Our framework comprises of five modular components (see Figure 1), where each stage focuses on a transformation of the data, from data collection to labeling:

1. A web scraper that collects data, images, and floor plans;
2. An image processor powered by LLaVA [28];
3. A GeoJSON and inspection note generator using OpenAI's GPT-4.1-mini [29];
4. An EnergyPlus[1] [30] simulation; and
5. A labeling system that combines heuristic rules with GPT-based natural language inference.

While our pipeline is tailored to generate labeled data from images and tabular data, it is inherently modular and extensible. Any stage is easily modified or expanded for other related purposes, and different information can be generated in addition to or in place of any data produced by this pipeline. Rather than proposing a rigid set of steps, we present a flexible framework

[1] EnergyPlus™ is a trademark of the United States Department of Energy.

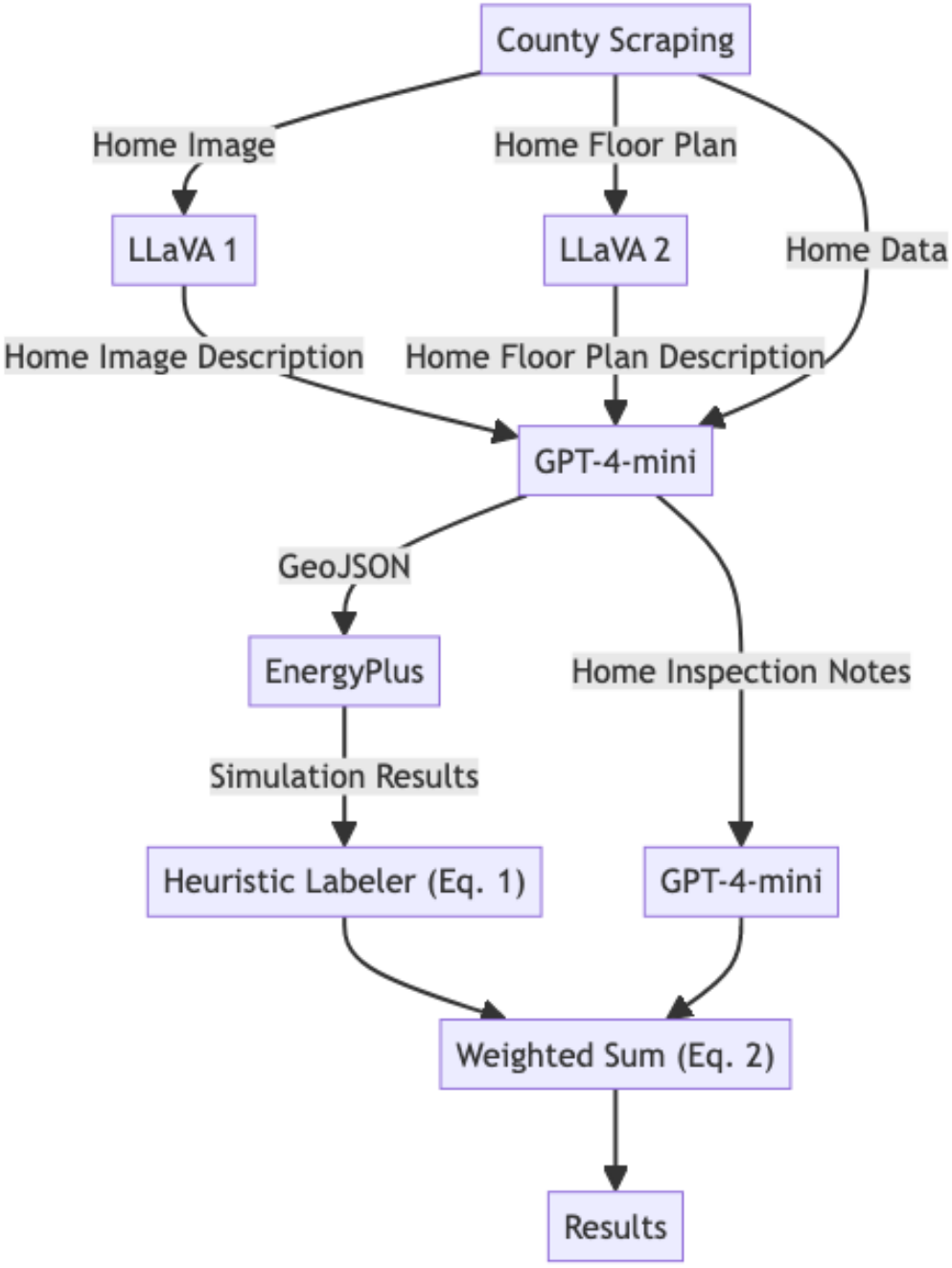

Figure 1: Overview of our proposed pipeline.

that integrates generative AI, web scraping, and building simulation, designed for rapid, low-cost data generation in building energy and other fields that traditionally suffer from data scarcity. Ultimately, the data generated by our framework can be used to prototype, design, train, and research urban energy systems.

An instance of this pipeline was implemented and executed[2] on a `g3.medium` flavor JetStream 2 virtual machine running Ubuntu 24.04.2 (Noble). Specifically, the system featured one NUMA node with 8 AMD EPYC-Milan processors, 30 GB of RAM, and an NVIDIA A100 SXM4 40 GB GPU (of which 10 GB was allocated). Additionally, it was fully virtualized (KVM and AMD-V). To run the pipeline, we paid $0.36 (USD) for OpenAI requests to produce data for 257 homes—about $0.0014 per home. We used the PyTorch [31] machine learning framework, and the Hugging Face Transformers library [32] to load the models we used. In the subsections that follow, we describe each pipeline component in detail.

2.1. Scraping the Data

To ensure the the synthetic data we generated reflects real-world homes, we grounded it in data collected from county datasets. Specifically, we gathered data from Northampton County, Pennsylvania, where two of the authors work and reside. To collect this data, we implemented a web scraper using `Selenium WebDriver` [33] and `ChromeDriver` [34]. For each residential property on each street in the list of streets to process, the scraper extracts key attributes, such as number of rooms, total floor area, and other metadata listed in Table 1. This data is saved to a JSON file for each home. Additionally, the scraper downloads two images: a street view photograph and a floor plan, both of which are made available on the County's public-facing platform. An example of each is depicted in Figure 2.

2.2. Processing Images

After scraping the images and floor plans from the county portal, they are analyzed using LLaVA [28]. This step processes the images to translate them into a textual description. For example, the floor plans can be used to define the geometry of the home, and the image to determine the quality

[2]Our source code is available at: `https://github.com/Lafayette-EshbaughSilveyra-Group/synthetic-homes`.

Collected Data	**Type**
Year Built	Year
Remodeled Year	Year
Land Use Code	String
Total Square Feet Living Area	Number
Number of Stories	Number
Grade	String
CDU	String
Building Style	String
Total Rooms	Number
Bedrooms	Number
Full Baths	Number
Half Baths	Number
Additional Fixtures	Number
Total Fixtures	Number
Heat/Air Cond	String
Heating Fuel Type	String
Heating System Type	String
Attic Code	String
Unfinished Area	Number
Rec Room Area	Number
Finished Basement Area	Number
Fireplace Openings	Number
Fireplace Stacks	Number
Prefab Fireplaces	Number
Basement Garage (Number of Cars)	Number
Condo Level	Number
Condo/Townhouse Type	String
Basement	String
Exterior Wall Material	String
Physical Condition	String
Sketch Data	Dictionary of floorplan segment areas

Table 1: All data we collected from the county portal. Not all homes have values for each variable.

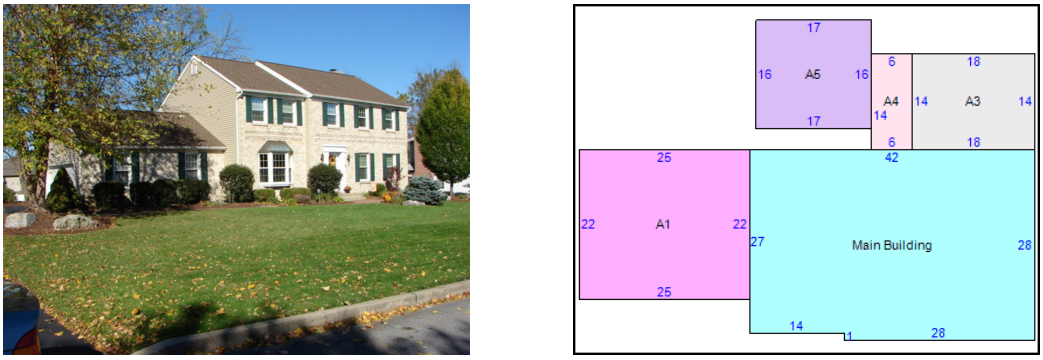

Figure 2: An example image and floor plan from the Northampton County database.

of the windows. The use of images allows our pipeline to infer important aspects of the homes that will be used to generate the GeoJSON, which is ultimately used to generate the IDF file required by EnergyPlus.

The image processing step originally was conducted using GPT. However, our experiments (see Section 3.1) displayed lack of detail in the analyses produced by that model. We pivoted to LLaVA and found that it outperformed GPT in every experiment. We hypothesize that this advantage stems from LLaVA's architecture: it employs an early fusion design in which images are converted into visual tokens by CLIP [35] that are then prepended to the textual prompt [28]. These visual tokens are passed through the transformer layers of the LLM together with text tokens, enabling multimodal attention at every layer. It has been demonstrated that vision tokens are most critical for a model in early layers, when they fuse into text tokens [36]. A likely result of this is the reduction of the model's sensitivity to variations in the image, which may explain its stronger performance in our experiments.

While GPT-4V (GPT's vision model) is proprietary, the case can be made that it possesses a different structure. Evaluation studies show that it performs well across visual reasoning and captioning tasks, but it falls short in fine grained visual problems, requiring complex visual tasks to be broken up into interleaved subfigures and text [37]. These evaluations are similar to evaluations from late fusion (connector) models. For example, BLIP-2 shows strengths in captioning images and instruction-following, while it is less robust with fine-grained spatial reasoning [38]. Another model, MiniGPT-4, demonstrates a similar profile: it has strengths in tasks such as image description, but falters with complex spatial reasoning [39]. Both BLIP-2 and MiniGPT-4 are late fusion models, where compressed visual features are

routed into the LLM at later stages [38, 39]. As shown, BLIP-2, MiniGPT-4, and GPT-4V all suffer from a very similar weakness: fine-grained or complex spatial reasoning. Based on this similarity, we hypothesize that GPT-4V is also a late fusion model. This helps explain why GPT performed differently from LLaVA in our experiments: as structure dictates function, differences in behavior strongly suggest differences in design. On the basis of this analysis, we feel confident to select LLaVA to complete this task.

2.3. Generating GeoJSON

Once the images are processed, we utilize the descriptions given by LLaVA in a GPT prompt to generate a GeoJSON file and home inspection notes. The prompt provides the image descriptions (Section 2.2) and data that was scraped from the county portal (Section 2.1) and directs the model to take two actions:

- The prompt instructs the model to generate a GeoJSON file for the building, including geometry, data from the county, and five estimated performance perimeters. These estimated parameters, defined according to standard convention, include the HVAC heating and cooling coefficients of performance, r-values for the roof and wall, and the air change rate.

- The prompt directs GPT to write a short inspection note, focused on energy-related observations such as insulation, HVAC type/age, visible windows, and any inferred upgrades. This inspection note is placed in the GeoJSON file.

The prompt contains strict guidelines to ensure outputs are valid, accurate, and complete. An excerpt from an example GeoJSON object is provided in Figure 3.

We use GPT for structured data generation given its strong ability to produce well-formed JSON outputs from descriptive prompts. Multiple studies have shown that LLMs perform well on generation tasks under strict schema constraints, even with no previous prompting or fine tuning. For example, StructuredRAG's benchmark suite showed 82% format compliance under JSON prompt conditions [40]. As we built the pipeline, we reviewed GPT's responses and it seldom failed to adhere to the JSON structure. In the rare case that it doesn't, our program catches the JSON error and automatically reprompts GPT for that example.

```
{
  "type": "Feature",
  "properties": {
    "name": "Generated Home",
    "floor_area": 2576,
    "building_type": "Single family",
    "inspection_note": "...",
    "hvac_heating_cop": 0.85,
    "hvac_cooling_cop": 3.0,
    "wall_r_value": 13,
    "roof_r_value": 30,
    "air_change_rate": 0.35
  },
  "geometry": {
    "type": "Polygon",
    "coordinates": [...]
  }
}
```

Figure 3: Excerpt of a generated GeoJSON file.

2.4. Running EnergyPlus Simulations

To execute a simulation in EnergyPlus, we take the GeoJSON generated by GPT (Section 2.3) and convert it to an IDF file for use in EnergyPlus. We use a template IDF file, filled with default values that are replaced with variables from the GeoJSON data, such as the geometry, HVAC heating and cooling coefficients of performance, r-values for the wall and roof, and the air change rate. Additionally, the template has many fields with constant values, such as the simulation running period and materials, constructions, and zones used in the simulation. Once the details from the GeoJSON are copied into the template, a final IDF file is produced.

The templating process is facilitated with the `eppy` package [41], which makes programmatic IDF generation straightforward. Then, we use ExpandObjects to prepare the file for simulation. ExpandObjects is bundled with EnergyPlus, and its primary use case is to take an IDF and expand template objects—such as the `HVACTemplate` we use—into full systems [42]. Finally, we run the expanded IDF file through EnergyPlus, producing final simulation results.

2.5. Determining Energy Efficiency of Homes

The energy efficiency of homes is measured using two components: (1) HVAC and insulation efficiency and (2) inspection notes. The first component is derived from the EnergyPlus simulation results (Section 2.4), while the second component is generated using GPT (Section 2.3). To prepare the data, we take the results from each EnergyPlus simulation and corresponding the home inspection note and label them using two scores. The first score pertains to the HVAC system, while the second score pertains to insulation. The process of computing these scores requires three steps:

1. Rate the need of replacing or improving HVAC systems and/or insulation by using GPT to parse the home inspection notes. We refer to this score as λ and its value is in $[0, 1]$.
2. Calculate a heuristic score for HVAC systems and/or insulation based on the EnergyPlus simulation results. This score (η) is computed using Equation 1.

$$\eta = \frac{\alpha - \beta}{\gamma - \beta} \tag{1}$$

   where α is the measured value of the home being scored, β represents the home that is the most efficient for each retrofit category, and γ represents the home that is the least efficient for each retrofit category. For example, suppose homes H_1, H_2, H_3, and H_4 consume $\alpha_1 = 4000$ kWh, $\alpha_2 = 10000$ kWh, $\alpha_3 = 5000$ kWh, and $\alpha_4 = 7000$ kWh with their HVAC systems, respectively. Then, $\beta = 4000$ kWh and $\gamma = 10000$ kWh, meaning H_1 scores 0.000, H_2 scores 1.000, H_3 scores 0.166, and H_4 scores 0.500. In this scenario, H_2 and H_4 would be prioritized for HVAC retrofitting, since they offer greater potential energy savings.
   This naïve formula is not the only option; it can be replaced for other formulas that score the EnergyPlus simulation results. A modified version of the logic above could incorporate additional weights which reflect size, age, or a combination of these and other variables.
3. Create a numerical rating (μ) by normalizing the combined results from steps 1 and 2. This is calculated by taking the weighted average of λ and η, as depicted in Equation 2.

$$\mu = \frac{.80\eta + .20\lambda}{2} \tag{2}$$

We weigh the GPT text score at 20% and the EnergyPlus heuristic rating at 80%, since GPT is much more sensitive than the heuristic function (see Section 3.2 for more).

We write the inspection notes, EnergyPlus simulation results, and labels for each example into one JSONL file.

This completes our end-to-end dataset generation process, yielding a unified dataset that combines textual and simulation-based information with consistent labeling. By design, each component of the pipeline can be adapted, replaced, or extended for use in other domains or research questions, making the framework a reusable foundation for diverse modeling and simulation tasks.

3. Experiments & Results

There is great risk that tools used within the pipeline could impact the results due to their architecture. To mitigate some of those concerns, we conducted experiments that validate the output produced by our pipeline according to the input received. Two of the main areas that showed the greatest bias in our pipeline were the image processing component from Section 2.2 and the labeler from Section 2.5. Some of these tests were executed on Lafayette College's high-performance computing cluster, Firebird, while others were run on a local machine. In the following subsections we address each case.

3.1. Evaluating Visual Focus with Occlusion Testing

In image processing, it is crucial that only key portions of the images in question trigger differences in the response of a model. We refer to this as *focus*. For example, if the prompt asks about the state of the roof of a home, the tree next to the home should be inconsequential in comparison to the roof itself. To evaluate this, we use a technique called Occlusion.

Occlusion measures the necessity of a part of an image: if removing a feature causes the prediction to change, that feature was necessary for the model's decision [43, 44]. When we remove image portions, we replace them with a neutral value, such as black. This creates a masked version of the image. The degree of change measured between the model's output for this masked image and its baseline response reflects the importance of the masked cell. High sensitivity to the removal of a feature suggests the model relied

heavily on that region to produce its output, indicating that the region was internally necessary to the model's decision process.

To compare the focus of the GPT and LLaVA LLMs when analyzing images, we ran occlusion tests. We provided the models with twenty different images of homes: ten with roofs showing no signs of damage, and ten with roofs with significant damage. Each model was instructed to evaluate and describe the state of the roof and justify its evaluation. We first took a baseline where no part of the image was masked. Then, the image was divided into one hundred cells, a number we selected to balance effectiveness, efficiency, and cost. Each cell of the image was masked, and the model was executed on the original prompt and this new image. Textual responses were embedded into vectors using the `all-MiniLM-L6-v2` SentenceTransformers model [45], a lightweight and widely used model sufficient for obtaining sentence-level numerical representations. Then, to measure the difference between each execution of the experiment, we took the cosine distance of each embedded response from the baseline. Additionally, heatmaps of these differences were assembled using `matplotlib` [46].

The mean difference value in roof cells and non-roof cells for each image was calculated. Figure 4 depicts the distribution of the forward occlusion results. These scatter plots are particularly telling—GPT (Figure 4a) evenly scatters the data points on either side of the line $y = x$, indicating GPT has no preference for which area in the image is considered important. In comparison, LLaVA (Figure 4b) tends to produce results in the upper half of the graph. This illustrates LLaVA's improvement over GPT plainly: more often than not, LLaVA's response depends more on the roof than not.

Additionally, overall means and standard deviations were calculated for GPT and LLaVA (Figure 5). In a well-focused model, the mean difference in the relevant area should be greater than the mean difference anywhere else. This behavior occurs since relevant cells should account for the majority of the response given by the model. In our experiments, we observe that GPT reports identical roof and non-roof mean differences (Figure 5a). However, LLaVA achieved a roof mean difference approximately 20% greater than its non-roof mean difference (Figure 5b).

When we compared individual GPT and LLaVA occlusion results, we found more evidence that LLaVA performs better at focusing on key parts of the images. LLaVA is much more particular about which cells are key to construct the response; GPT produces results that look stochastic. Figure 6 displays one noteworthy example—LLaVA focuses on a more specific section

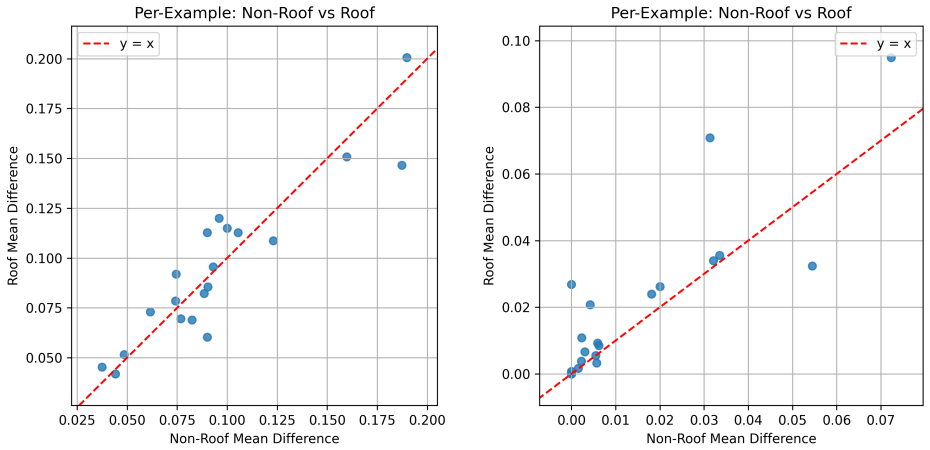

(a) GPT results.

(b) LLaVA results.

Figure 4: GPT and LLaVA forward occlusion per image results.

	Mean Difference	SD
Roof	0.0956	0.0384
Non-Roof	0.0956	0.0408

(a) GPT forward occlusion overall statistics

	Mean Difference	SD
Roof	0.0208	0.0241
Non-Roof	0.0149	0.0197

(b) LLaVA forward occlusion overall statistics

Figure 5: Forward occlusion statistics for GPT and LLaVA.

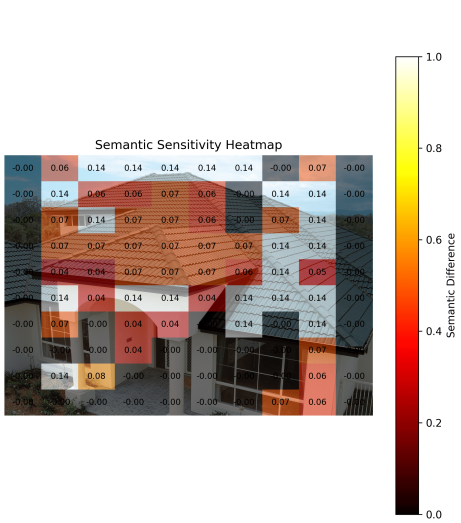

(a) LLaVA occlusion results. These results show less sensitivity and more focus on the more important parts of the image.

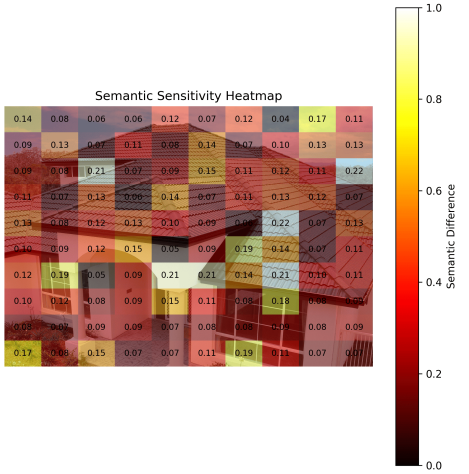

(b) GPT occlusion results. These results demonstrate extreme sensitivity to the image, which is not desired. This sensitivity means the model focuses less on the most important parts of the image while responding to the prompt.

Figure 6: GPT and LLaVA occlusion results.

of the image, primarily consisting of the home's roof. GPT, on the other hand, behaves much more randomly. Based on these results, we selected LLaVA for use in the image processing step of our pipeline. Full experimental details and findings are available in Appendix B.

3.2. Validation of Labeling Components

As discussed in Section 2.5, the pipeline includes a labeler that quantifies the efficiency of homes. The labeler consists of two components: a labeler for the EnergyPlus simulation results and a labeler for the home inspection notes. Our goal is to achieve a labeler whose outputs are meaningful, and that balances the contributions of each component. In our study, we conducted an experiment to measure the sensitivity of each component. Given the multimodal nature of our pipeline, the first two parts of this experiment employ Ablation, with the third building on the findings of the original two.

Ablation testing is commonly used to evaluate multimodal models by focusing on one modality at a time [47]. It can reveal biases, weak model components, and hallucinations by fixing all but one of a model's modality inputs and varying the unfixed one. Biases could impact a labeling module like ours by considering certain modalities of the data more important than

others. This can have a negative effect on the overall labels assigned, as some of the data within the dataset is used less—or perhaps not used at all—to label the dataset.

We applied two ablation tests to reveal any biases between the EnergyPlus simulation results and inspection note components in our labeling model. Each test varied the efficiency of the home in one component, keeping the other component constant. Results were plotted to show the variation in the output given the efficiency of the varied component. To complement the ablation tests, we ran an additional test in which we paired every possible combination of home inspection notes and simulation results representing efficient and inefficient homes. For each prompt, we ran five trials, and the mean and standard deviation are reported. Full experimental values are provided in Appendix A. We present three versions of the labelers, iteratively mitigating bias in each.

3.2.1. Naïve Labeler

Originally, we used GPT to generate the labels, feeding it both the simulation data and the inspection notes. However, we found that this architecture was heavily skewed toward the inspection notes, such that those features disproportionally determined the label output, even when paired with simulation data (see Figure 7). This skew is especially evident when viewing the text ablation results (Figure 7a) and the combined variation results (Figure 7c). In the text ablation results, as the inspection notes move from very inefficient (HVAC 1) to very efficient (HVAC 5), there is a dramatic reduction in score. Clearly, the labeler is extremely sensitive to text. However, it is much less sensitive to simulation results. In fact, in the EnergyPlus ablation test (Figure 7b), we would expect mean HVAC label values to trend to decrease as the index increases, since as index increases, COP also increases. Yet this trend does not occur; instead mean HVAC label values fluctuate. This bias perpetuates into the combined variation tests, which show a clear favoring of text data.

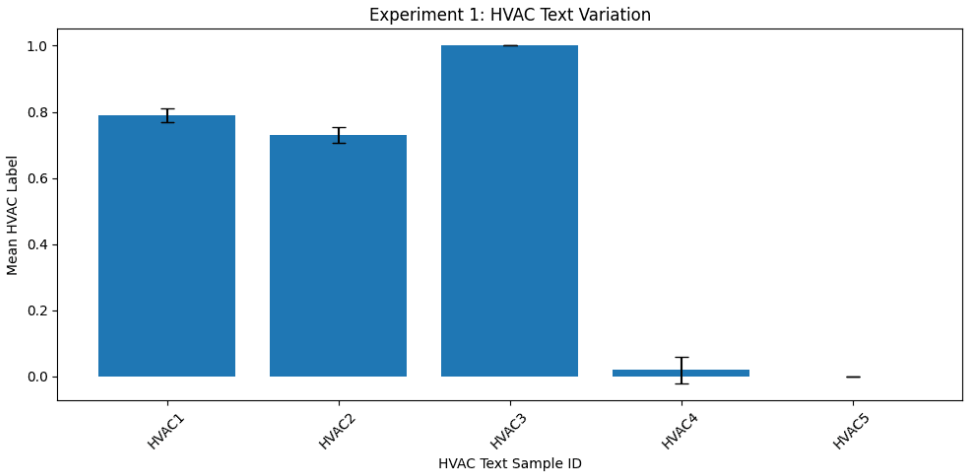

(a) Ablation testing with varying text samples.

Figure 7: Ablation and combined variation testing of the labeling module using only GPT.

3.2.2. Heuristic Labeler

To reduce bias, we introduced the heuristic labeler. GPT processes the text and a heuristic labeler processes the simulation data, using the heuristic labeling equations described in Section 2.5. The results of this iteration—displayed in Figure 8—were an advancement from the previous. We observed the desired decreasing trend in the EnergyPlus ablation test (Figure 8b). At this stage, EnergyPlus results reflected the inputs; with an increase in COP, the HVAC score decreases. In the combined variation test (Figure 8c), we observed that the HVAC scores given were high when the inspection note described an inefficient home, and low when it described an efficient home; the heuristic labels were still lightly weighted in comparison to GPT's inspection note labels. The current results do not produce a labeler where an input describing a home that is efficient in a given category and paired with inefficient simulation data produces a result similar to an input describing an inefficient home paired with efficient simulation data. In other words, the two middle results of any combined variation test, like the ones presented in Figure 8c, should have a similar mean label value.

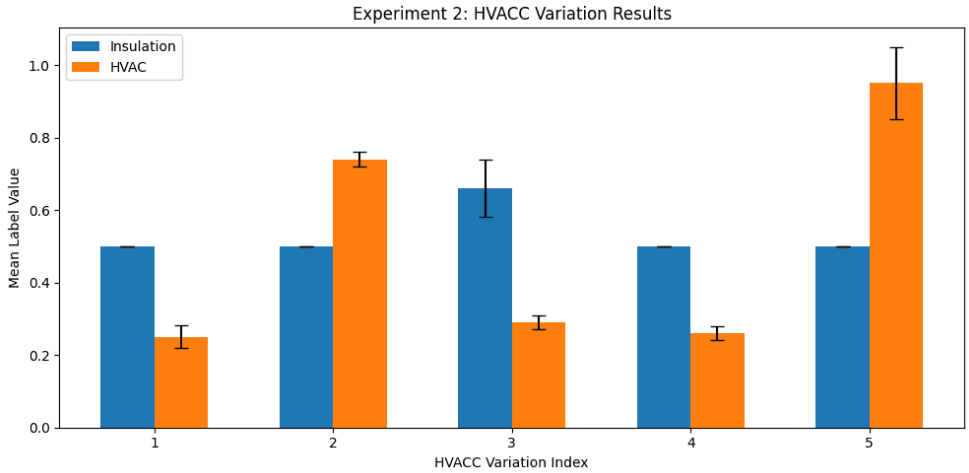

(b) Ablation testing with varying EnergyPlus simulation results. As the index increases, COP also increases.

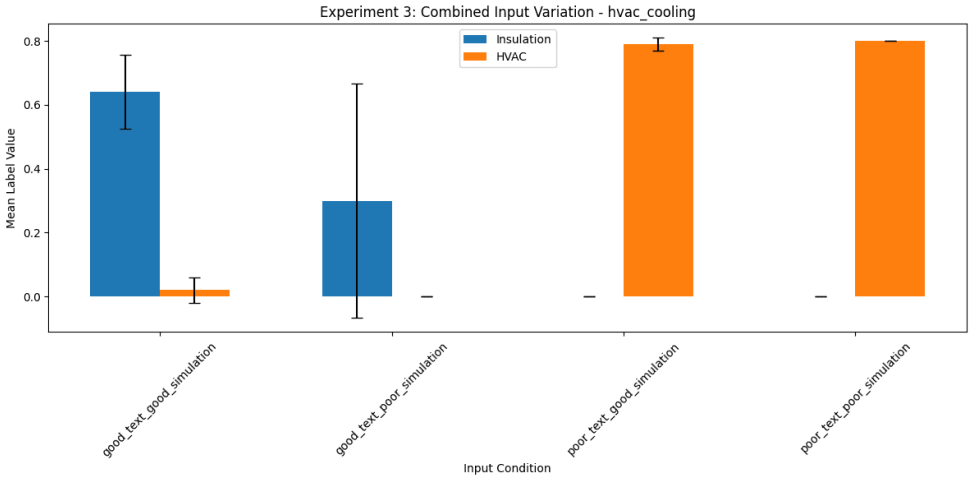

(c) Combined variation testing using the `hvac_cooling` variable. Regardless of the simulation results, good text brings a low recommendation, and bad text brings a high recommendation. Therefore, the labeler in this state is strongly biased toward text data.

Figure 7: Ablation and combined variation testing of the labeling module using only GPT (continued).

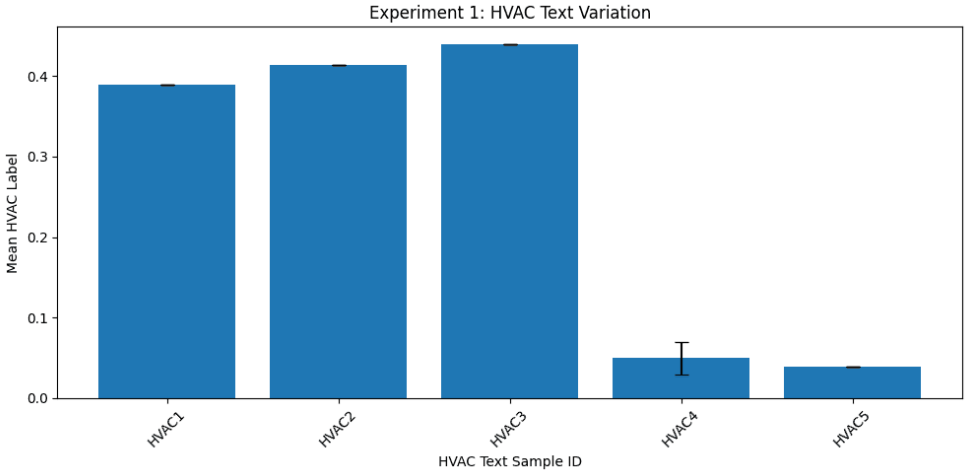

(a) Ablation testing with varying text samples.

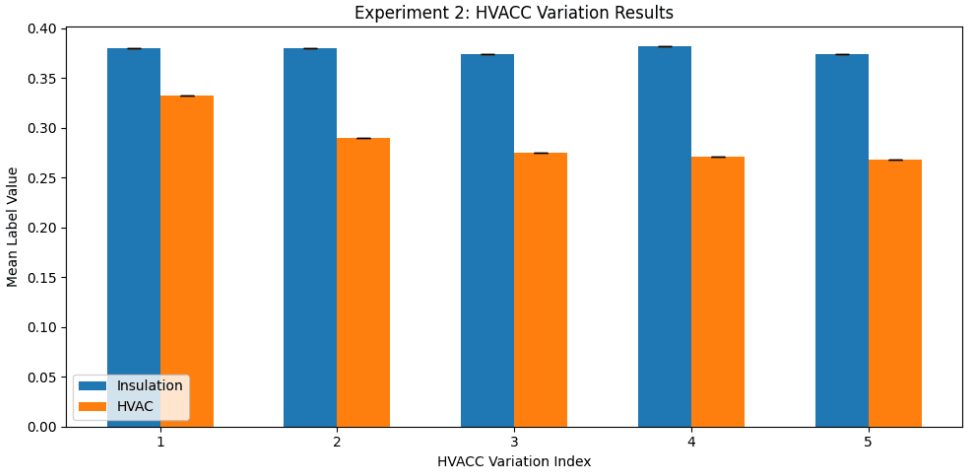

(b) Ablation testing with varying EnergyPlus simulation results. As the index increases, COP also increases.

Figure 8: Experimental results after introducing the heuristic labeler.

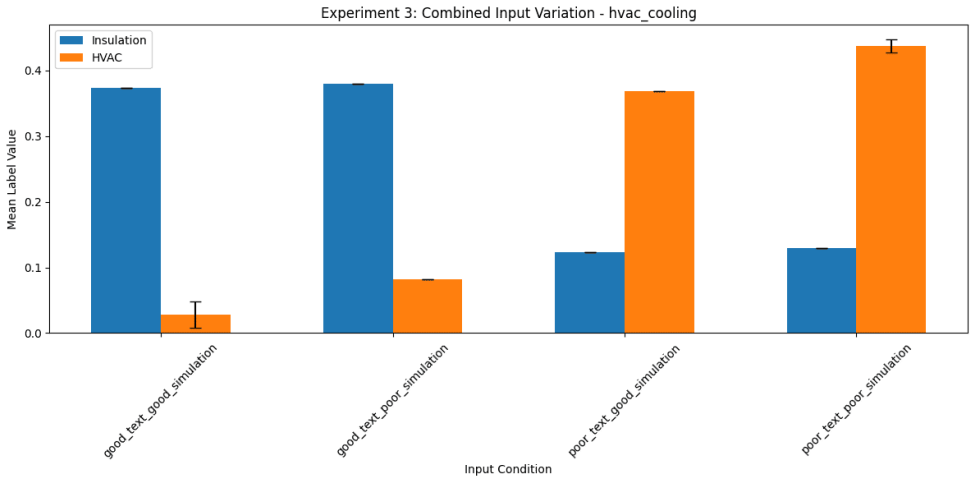

(c) Combined variation testing using the `hvac_cooling` variable.

Figure 8: Experimental results after introducing the heuristic labeler (continued).

3.2.3. Weighted Heuristic Labeler

To balance the weights between text and simulation data, we employ a weighted sum. The text score is weighed at 20% and the simulation results at 80%. With this updated methodology, our results are more equitable (see Figure 9). The EnergyPlus ablation test (Figure 9b) showed a much more pronounced decreasing trend, and combined variation tests (Figures 9c and 9d) reveal that the model more equally weighs between the two modalities. For both HVAC- and insulation-related variables, in combined input variation testing, we observed that inspection notes and data describing efficient homes scored the lowest, notes and data describing inefficient homes scored the highest, and mixed-efficiency notes and data scored between the previous values. Therefore, the labeler now accurately assigns reasonable retrofits.

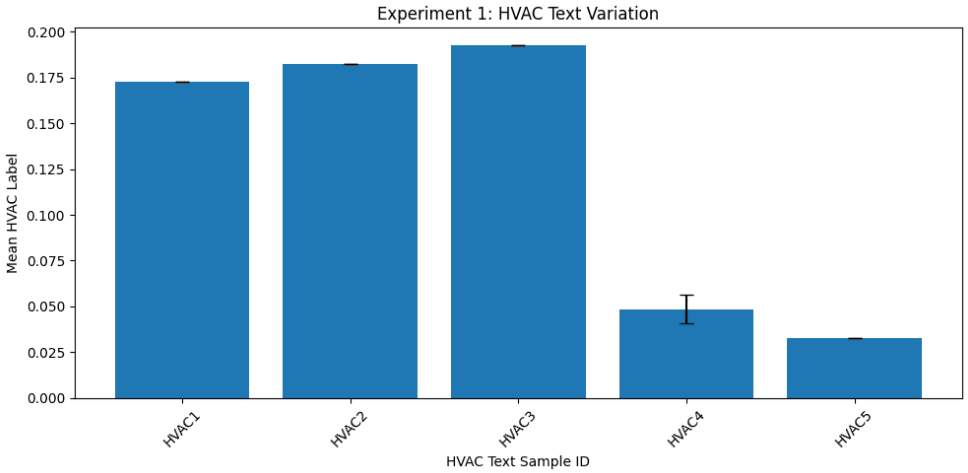

(a) Ablation testing with varying text samples.

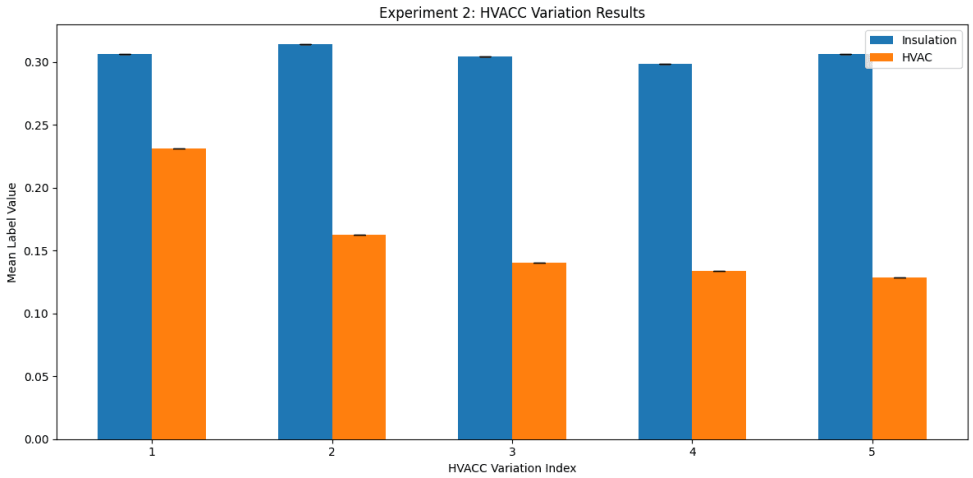

(b) Ablation testing with varying EnergyPlus simulation results. Varying the `hvac_cooling` variable.

Figure 9: Experimental results after introducing the weighted sum.

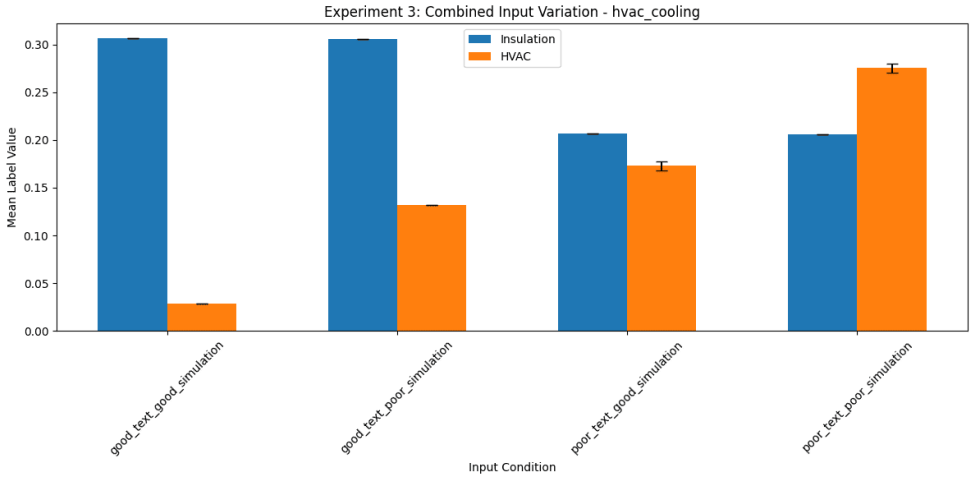

(c) Combined variation testing using the `hvac_cooling` variable.

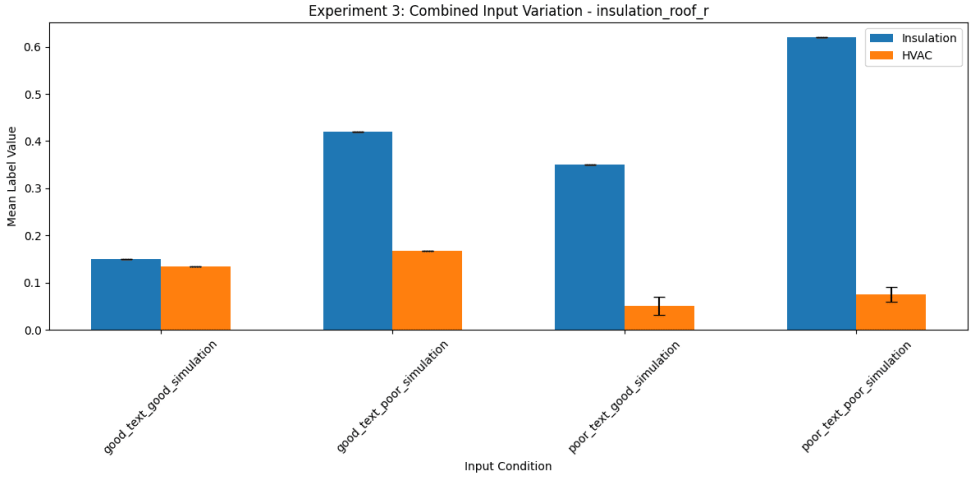

(d) Combined variation testing using the `insulation_roof_r` variable.

Figure 9: Experimental results after introducing the weighted sum (continued).

4. Conclusion

The experiments in Section 3 demonstrate a level of confidence above previous work such as Zhang *et al.* [19] and Xiao and Xu [20]. These works and others either accept the output of the LLMs or use procedural evaluation techniques. Occlusion and ablation offer stronger empirical support that the

image processing and labeling components of our pipeline—which are both LLM-based—perform as expected. Our results directly address and mitigate concerns about hallucination and unreliability raised in prior work [24]. It is right to be skeptical of LLMs and other ML models—but with our results, we clearly demonstrate our pipeline is not as susceptible to some of the issues Liu *et al.* raise.

In this work, we presented a novel way to generate data for urban energy research and other fields that use similar data. Using a multimodal pipeline, we produce this labeled data in a cost-effective and efficient way. We also performed an in depth analysis to ensure that our generative AI pipeline components were behaving as expected, taking into account the concerns of Liu.

Generative AI is a powerful tool, and we recognize the importance of this new frontier as described by Xu *et al.* [17] and Liu. Not only does our work demonstrate a step forward in the urban energy field, it also presents a useful, malleable tool that experts and researchers can use for a variety of tasks.

Consequently, there is much work that can utilize or expand upon this study. One promising direction is the use of this pipeline to train machine learning algorithms. With the pipeline introduced here, one could create a neural network that recommends energy efficiency retrofits based on multimodal data.

Overall, the high prices, lack of availability, or privacy concerns attached to the collection of urban energy data can be avoided by generating synthetic data. With our framework, all of these concerns are alleviated and realistic, labeled data is produced. This reduced dependence on costly or restricted data sources provides a pathway towards more accessible and reproducible research.

Acknowledgments

The authors extend gratitude to Lafayette College for supporting this work by funding it through the EXCEL Scholars program and providing computational resources with the Firebird high performance computing cluster. Access to the JetStream2 system was made possible via the NSF-funded ACCESS program, facilitated by Lafayette College. We also thank to the NSF, ACCESS for supporting this resource, and to Indiana University for hosting JetStream2 as a part of the ACCESS program.

CRediT Author Attributions

Jackson Eshbaugh: Software, Investigation, Writing - Original Draft, Visualization, Validation, Data Curation. **Chetan Tiwari**: Conceptualization, Writing - Review and Editing, Supervision (supporting). **Jorge Silveyra**: Conceptualization, Writing - Review and Editing, Methodology, Supervision (lead), Project Administration, Validation

Glossary

Ablation A test used to evaluate multimodal models by observing how a model's output responds to each varying modality.

EnergyPlus A versatile building energy modeling tool provided by the United States Department of Energy. Orginally published in 2002.

GPT A popular large language model by OpenAI with a wide variety of uses.

LLaVA An LLM integrated with CLIP, OpenAI's visual model. Introduced by Liu *et al.* in 2023.

Occlusion A test commonly used to evaluate visual machine learning models by blocking out parts of an image and comparing to a baseline.

Acronyms

AI Artificial Intelligence

COP Coefficient of Performance

GeoJSON Geographic JSON

IDF Input Definition File

JSON JavaScript Object Notation

JSONL JSON Lines

LLM Large Language Model

ML Machine Learning

References

[1] U.S. Energy Information Administration, Drivers of U.S. household energy consumption, 1980–2009, Tech. rep., U.S. Department of Energy, https://www.eia.gov/analysis/studies/buildings/households/ (Feb. 2015).

[2] U.S. Environmental Protection Agency, Climate Change Indicators: Residential Energy Use, https://www.epa.gov/climate-indicators/climate-change-indicators-residential-energy-use (Jan. 2025).

[3] E. F. Bompard, S. Conti, M. J. Masera, G. G. Soma, A New Electricity Infrastructure for Fostering Urban Sustainability: Challenges and Emerging Trends, Energies 17 (22) (2024) 5573. doi:10.3390/en17225573.

[4] A. Perera, K. Javanroodi, V. M. Nik, Climate resilient interconnected infrastructure: Co-optimization of energy systems and urban morphology, Applied Energy 285 (2021) 116430. doi:10.1016/j.apenergy.2020.116430.

[5] Y. Zeng, Y. Cai, G. Huang, J. Dai, A Review on Optimization Modeling of Energy Systems Planning and GHG Emission Mitigation under Uncertainty, Energies 4 (10) (2011) 1624–1656. doi:10.3390/en4101624.

[6] A. Hajri, R. Garay-Marinez, A. M. Macarulla, M. A. Ben Sassi, Data-driven model for heat load prediction in buildings connected to district heating networks, Energy 329 (2025) 136684. doi:10.1016/j.energy.2025.136684.

[7] U.S. Department of Energy, Getting Started (3 2025).
URL https://energyplus.net/assets/nrel_custom/pdfs/pdfs_v25.1.0/GettingStarted.pdf

[8] D. Wan, X. Zhao, W. Lu, P. Li, X. Shi, H. Fukuda, A Deep Learning Approach toward Energy-Effective Residential Building Floor Plan Generation, Sustainability 14 (13) (2022) 8074. doi:10.3390/su14138074.

[9] M. H. Elnabawi, N. Hamza, A Methodology of Creating a Synthetic, Urban-Specific Weather Dataset Using a Microclimate Model for Building Energy Modelling, Buildings 12 (9) (2022) 1407. doi:10.3390/buildings12091407.

[10] S. Lee, J. Cha, M. K. Kim, K. S. Kim, V. H. Pham, M. Leach, Neural-Network-Based Building Energy Consumption Prediction with Training Data Generation, Processes 7 (10) (2019) 731. doi:10.3390/pr7100731.

[11] M. H. Zweig, G. Campbell, Receiver-operating characteristic (ROC) plots: A fundamental evaluation tool in clinical medicine, Clinical Chemistry 39 (4) (1993) 561–577. doi:10.1093/clinchem/39.4.561.

[12] A. C. J. W. Janssens, F. K. Martens, Reflection on modern methods: Revisiting the area under the ROC Curve, International Journal of Epidemiology 49 (4) (2020) 1397–1403. doi:10.1093/ije/dyz274.

[13] F. Stinner, M. Wiecek, M. Baranski, A. Kümpel, D. Müller, Automatic digital twin data model generation of building energy systems from piping and instrumentation diagrams (Aug. 2021). arXiv:2108.13912, doi:10.48550/arXiv.2108.13912.

[14] S. Agostinelli, F. Cumo, G. Guidi, C. Tomazzoli, Cyber-Physical Systems Improving Building Energy Management: Digital Twin and Artificial Intelligence, Energies 14 (8) (2021) 2338. doi:10.3390/en14082338.

[15] A. Francisco, N. Mohammadi, J. E. Taylor, Smart City Digital Twin–Enabled Energy Management: Toward Real-Time Urban Building Energy Benchmarking, Journal of Management in Engineering 36 (2) (2020) 04019045. doi:10.1061/(ASCE)ME.1943-5479.0000741.

[16] M. Belik, O. Rubanenko, Implementation of Digital Twin for Increasing Efficiency of Renewable Energy Sources, Energies 16 (12) (2023) 4787. doi:10.3390/en16124787.

[17] H. Xu, F. Omitaomu, S. Sabri, S. Zlatanova, X. Li, Y. Song, Leveraging generative AI for urban digital twins: A scoping review on the autonomous generation of urban data, scenarios, designs, and 3D city models for smart city advancement, Urban Informatics 3 (1) (2024) 29. doi:10.1007/s44212-024-00060-w.

[18] S. Dodge, J. Xu, B. Stenger, Parsing floor plan images, in: 2017 Fifteenth IAPR International Conference on Machine Vision Applications (MVA), IEEE, Nagoya, Japan, 2017, pp. 358–361. doi:10.23919/MVA.2017.7986875.

[19] L. Zhang, V. Ford, Z. Chen, J. Chen, Automatic Building Energy Model Development and Debugging Using Large Language Models Agentic Workflow, preprint (2024). doi:10.2139/ssrn.4864703.

[20] T. Xiao, P. Xu, Exploring automated energy optimization with unstructured building data: A multi-agent based framework leveraging large language models, Energy and Buildings 322 (2024) 114691. doi:10.1016/j.enbuild.2024.114691.

[21] Y. Lin, Y. Yao, J. Zhu, C. He, Application of Generative AI in Predictive Analysis of Urban Energy Distribution and Traffic Congestion in Smart Cities, in: 2025 IEEE International Conference on Electronics, Energy Systems and Power Engineering (EESPE), IEEE, Shenyang, China, 2025, pp. 765–768. doi:10.1109/EESPE63401.2025.10987500.

[22] Z. Sha, W. Yue, S. Wang, N. Cheng, J. Wu, C. Li, Generative AI-Enabled Sensing and Communication Integration for Urban Air Mobility, in: 2024 IEEE 99th Vehicular Technology Conference (VTC2024-Spring), IEEE, Singapore, Singapore, 2024, pp. 1–5. doi:10.1109/VTC2024-Spring62846.2024.10683276.

[23] Y. Zhang, A. Schlüter, C. Waibel, SolarGAN: Synthetic Annual Solar Irradiance Time Series on Urban Building Facades via Deep Generative Networks (Jun. 2022). arXiv:2206.00747, doi:10.48550/arXiv.2206.00747.

[24] M. Liu, L. Zhang, J. Chen, W.-A. Chen, Z. Yang, L. J. Lo, J. Wen, Z. O'Neill, Large language models for building energy applications: Opportunities and challenges, Building Simulation 18 (2) (2025) 225–234. doi:10.1007/s12273-025-1235-9.

[25] F. Rehmann, M. Mosteiro-Romero, C. Miller, R. Streblow, Enhancing urban energy modeling: A case study of data acquisition, enrichment, and evaluation in Berlin, Energy and Buildings 346 (2025) 116070. doi:10.1016/j.enbuild.2025.116070.
URL https://linkinghub.elsevier.com/retrieve/pii/S037877882500800X

[26] T. Guo, M. Bachmann, M. Kersten, M. Kriegel, A combined workflow to generate citywide building energy demand profiles from

low-level datasets, Sustainable Cities and Society 96 (2023) 104694. doi:10.1016/j.scs.2023.104694.
URL https://linkinghub.elsevier.com/retrieve/pii/S2210670723003050

[27] D. Bishop, P. Gallardo, B. L. M. Williams, A Review of Multi-Domain Urban Energy Modelling Data, Clean Energy and Sustainability 2 (4) (2024) 10016–10016. doi:10.70322/ces.2024.10016.
URL https://www.sciepublish.com/article/pii/298

[28] H. Liu, C. Li, Q. Wu, Y. J. Lee, Visual Instruction Tuning (Dec. 2023). arXiv:2304.08485, doi:10.48550/arXiv.2304.08485.

[29] OpenAI, Introducing GPT-4.1 in the API, https://openai.com/index/gpt-4-1/ (Apr. 2025).

[30] D. B. Crawley, L. K. Lawrie, F. C. Winkelmann, W. Buhl, Y. Huang, C. O. Pedersen, R. K. Strand, R. J. Liesen, D. E. Fisher, M. J. Witte, J. Glazer, EnergyPlus: Creating a new-generation building energy simulation program, Energy and Buildings 33 (4) (2001) 319–331. doi:10.1016/S0378-7788(00)00114-6.

[31] J. Ansel, E. Yang, H. He, N. Gimelshein, A. Jain, M. Voznesensky, B. Bao, P. Bell, D. Berard, E. Burovski, G. Chauhan, A. Chourdia, W. Constable, A. Desmaison, Z. DeVito, E. Ellison, W. Feng, J. Gong, M. Gschwind, B. Hirsh, S. Huang, K. Kalambarkar, L. Kirsch, M. Lazos, M. Lezcano, Y. Liang, J. Liang, Y. Lu, C. K. Luk, B. Maher, Y. Pan, C. Puhrsch, M. Reso, M. Saroufim, M. Y. Siraichi, H. Suk, S. Zhang, M. Suo, P. Tillet, X. Zhao, E. Wang, K. Zhou, R. Zou, X. Wang, A. Mathews, W. Wen, G. Chanan, P. Wu, S. Chintala, PyTorch 2: Faster Machine Learning Through Dynamic Python Bytecode Transformation and Graph Compilation, in: Proceedings of the 29th ACM International Conference on Architectural Support for Programming Languages and Operating Systems, Volume 2, ACM, La Jolla CA USA, 2024, pp. 929–947. doi:10.1145/3620665.3640366.

[32] T. Wolf, L. Debut, V. Sanh, J. Chaumond, C. Delangue, A. Moi, P. Cistac, T. Rault, R. Louf, M. Funtowicz, J. Davison, S. Shleifer, P. Von Platen, C. Ma, Y. Jernite, J. Plu, C. Xu, T. Le Scao, S. Gugger, M. Drame, Q. Lhoest, A. Rush, Transformers: State-of-the-Art Natural Language

Processing, in: Proceedings of the 2020 Conference on Empirical Methods in Natural Language Processing: System Demonstrations, Association for Computational Linguistics, Online, 2020, pp. 38–45. doi:10.18653/v1/2020.emnlp-demos.6.

[33] Selenium, Selenium webdriver documentation, https://www.selenium.dev/documentation/webdriver/, accessed 2025-08-06 (Nov. 2024).

[34] Google, Chromedriver - webdriver for chrome, https://sites.google.com/chromium.org/driver/, accessed: 2025-08-06 (Jun. 2023).

[35] A. Radford, J. W. Kim, C. Hallacy, A. Ramesh, G. Goh, S. Agarwal, G. Sastry, A. Askell, P. Mishkin, J. Clark, G. Krueger, I. Sutskever, Learning Transferable Visual Models From Natural Language Supervision (Feb. 2021). arXiv:2103.00020, doi:10.48550/arXiv.2103.00020.

[36] S. Zhang, Q. Fang, Z. Yang, Y. Feng, LLaVA-Mini: Efficient Image and Video Large Multimodal Models with One Vision Token (Mar. 2025). arXiv:2501.03895, doi:10.48550/arXiv.2501.03895.

[37] Z. Yang, L. Li, K. Lin, J. Wang, C.-C. Lin, Z. Liu, L. Wang, The Dawn of LMMs: Preliminary Explorations with GPT-4V(ision) (Oct. 2023). arXiv:2309.17421, doi:10.48550/arXiv.2309.17421.

[38] J. Li, D. Li, S. Savarese, S. Hoi, BLIP-2: Bootstrapping Language-Image Pre-training with Frozen Image Encoders and Large Language Models (Jun. 2023). arXiv:2301.12597, doi:10.48550/arXiv.2301.12597.

[39] D. Zhu, J. Chen, X. Shen, X. Li, M. Elhoseiny, MiniGPT-4: Enhancing Vision-Language Understanding with Advanced Large Language Models (Oct. 2023). arXiv:2304.10592, doi:10.48550/arXiv.2304.10592.

[40] C. Shorten, C. Pierse, T. B. Smith, E. Cardenas, A. Sharma, J. Trengrove, B. van Luijt, StructuredRAG: JSON Response Formatting with Large Language Models (Aug. 2024). arXiv:2408.11061, doi:10.48550/arXiv.2408.11061.

[41] santoshphilip, Eppy, https://github.com/santoshphilip/eppy (Oct. 2024).

[42] U.S. Department of Energy, EnergyPlus Auxiliary Programs Documentation — Version 23.2.0, EnergyPlus, U.S. Department of Energy, see pages 45–48 for ExpandObjects preprocessor details (2023).
URL https://energyplus.net/assets/nrel_custom/pdfs/pdfs_v23.2.0/AuxiliaryPrograms.pdf

[43] S. Hooker, D. Erhan, P.-J. Kindermans, B. Kim, A Benchmark for Interpretability Methods in Deep Neural Networks (Nov. 2019). arXiv:1806.10758, doi:10.48550/arXiv.1806.10758.

[44] E. Balkir, I. Nejadgholi, K. Fraser, S. Kiritchenko, Necessity and Sufficiency for Explaining Text Classifiers: A Case Study in Hate Speech Detection, in: Proceedings of the 2022 Conference of the North American Chapter of the Association for Computational Linguistics: Human Language Technologies, Association for Computational Linguistics, Seattle, United States, 2022, pp. 2672–2686. doi:10.18653/v1/2022.naacl-main.192.

[45] N. Reimers, I. Gurevych, Sentence-BERT: Sentence Embeddings using Siamese BERT-Networks (Aug. 2019). arXiv:1908.10084, doi:10.48550/arXiv.1908.10084.

[46] T. M. D. Team, Matplotlib: Visualization with Python, Zenodo (May 2025). doi:10.5281/ZENODO.15375714.

[47] Y.-H. H. Tsai, S. Bai, P. P. Liang, J. Z. Kolter, L.-P. Morency, R. Salakhutdinov, Multimodal Transformer for Unaligned Multimodal Language Sequences (Jun. 2019). arXiv:1906.00295, doi:10.48550/arXiv.1906.00295.

Appendix A. Labeler Experimental Values

In this appendix, we list the detailed experimental values used to test the labeler in Section 3.2. Tables A.2 and A.3 give the text we used as home inspection notes. Table A.4 maps our EnergyPlus ablation test onto EnergyPlus variables, and Table A.5 shows the value that each index represents. Finally, Table A.6 gives the default values used in the EnergyPlus ablation test.

Any arbitrary simulation can be used for the textual ablation test and any arbitrary string for the EnergyPlus ablation test since both of these are

ID	Efficiency Level	Description
HVAC1	Very Inefficient	There is an older HVAC unit installed, with signs of rust on the exterior.
HVAC2	Inefficient	The HVAC system appears to be in working condition but is an older standard-efficiency model.
HVAC3	Moderate	The home uses window AC units rather than a central HVAC system.
HVAC4	Efficient	The HVAC system was recently replaced with a standard high-efficiency model and is expected to operate efficiently.
HVAC5	Very Efficient	A state-of-the-art HVAC system with smart thermostats and variable-speed compressors was recently installed, maximizing energy efficiency.

Table A.2: HVAC text descriptions by efficiency level.

constant and do not vary throughout the experiment. We pick an arbitrary simulation and use the neutral inspection note that follows:

> The home has two stories with vinyl siding and a shingled roof. Windows appear to be single-hung with no visible damage. The HVAC system is located on the first floor near the utility room. Insulation levels in the attic are unknown. Doors are wood-core with standard weather stripping.

Appendix B. Occlusion Results

In this appendix, we provide detailed information and results from our occlusion and reverse occlusion tests. Firstly, when running the test we utilized identical prompts for each model. For GPT, we prompted:

> You are a certified home inspector. Describe the status roof. Is it in good condition? Why or why not?

Likewise, we prompted LLaVA with the following:

ID	Efficiency Level	Description
INS1	Very Inefficient	Attic insulation is minimal, with exposed joists visible throughout, causing significant heat loss.
INS2	Inefficient	No signs of added insulation were observed in the basement ceiling, suggesting potential energy inefficiency.
INS3	Moderate	Walls appear to be adequately insulated based on construction year, though no upgrades were observed.
INS4	Efficient	Blown-in insulation is present in the attic to a depth of approximately 10 inches, providing good thermal resistance.
INS5	Very Efficient	High-performance spray foam insulation was installed throughout the walls, attic, and basement, providing maximum energy efficiency.

Table A.3: Insulation text descriptions by efficiency level.

Variable	Corresponding EnergyPlus Variable
WALLR	Wall R-value
ROOFR	Roof R-value
HVACH	HVAC Heating COP
HVACC	HVAC Cooling COP

Table A.4: A mapping from our ablation test variables to EnergyPlus variables.

Variable	1	2	3	4	5
WALLR	4.0	7.0	13.0	20.0	30.0
ROOFR	10.0	20.0	30.0	40.0	50.0
HVACH	0.7	0.8	0.9	0.95	1.0
HVACC	1.0	2.0	3.0	3.5	4.0

Table A.5: The values we used in our EnergyPlus ablation test.

Variable	Default Value
Air Change Rate	2.0
HVAC Heating COP	0.8
HVAC Cooling COP	3.0
Window U Value	2.0
Wall R Value	13.0
Roof R Value	30.0
HVAC System Type	Gas Furnace

Table A.6: The default values we used in our EnergyPlus ablation test.

> USER: <image>
> You are a certified home inspector. Describe the status roof. Is it in good condition? Why or why not? ASSISTANT:

These prompts differ slightly due to how the models are trained; namely, LLaVA expects an image token and labeled portions of the message. The majority of LLMs behave this way, and the GPT API likely wraps the given prompt in something similar.

In Table B.7, we provide our forward occlusion results, including roof mean difference (RMD) and non-roof mean difference (NRMD) values from both GPT and LLaVA and references to figures displaying GPT and LLaVA heatmaps side by side.

As noted in Section 3.1, we also ran reverse occlusion tests. While we didn't calculate quantitative values for these results, we attach them in Table **??**.

Metric	**1**	**2**	**3**	**4**	**5**	**6**	**7**	**8**	**9**	**10**
Damaged Roofs										
GPT RMD	0.0856	0.0920	0.0730	0.0689	0.1127	0.0453	0.0516	0.0603	0.1149	0.0419
GPT NRMD	0.0903	0.0745	0.0615	0.0824	0.0900	0.0375	0.0485	0.0900	0.1000	0.0442
LLaVA RMD	0.0033	0.0324	0.0949	0.0093	0.0262	0.0269	0.0356	0.0055	0.0038	0.0208
LLaVA NRMD	0.0057	0.0545	0.0723	0.0059	0.0200	0.0000	0.0335	0.0055	0.0022	0.0042
Roof Cells	70	80	53	83	97	96	80	96	91	88
Non-Roof Cells	30	20	47	17	3	4	20	4	9	12
Figure	B.10	B.11	B.12	B.13	B.14	B.15	B.16	B.17	B.18	B.19
Undamaged Roofs										
GPT RMD	0.1128	0.0785	0.1465	0.1508	0.0822	0.0956	0.1087	0.2005	0.0696	0.1200
GPT NRMD	0.1055	0.0742	0.1872	0.1598	0.0884	0.0930	0.1230	0.1898	0.0768	0.0959
LLaVA RMD	0.0709	0.0085	0.0007	0.0000	0.0340	0.0108	0.0066	0.0000	0.0017	0.0240
LLaVA NRMD	0.0313	0.0062	0.0000	0.0000	0.0321	0.0023	0.0030	0.0000	0.0015	0.0181
Roof Cells	53	47	68	49	81	39	70	60	47	73
Non-Roof Cells	47	53	32	51	19	61	30	40	53	27
Figure	B.20	B.21	B.22	B.23	B.24	B.25	B.26	B.27	B.28	B.29

Table B.7: Quantitative results from our forward occlusion experiments, including roof mean difference (RMD) and non-roof mean difference (NRMD) for both GPT and LLaVA. The number of cells in the image considered roof and non-roof are listed, and figures of side by side comparisons of the resulting heatmaps are referenced.

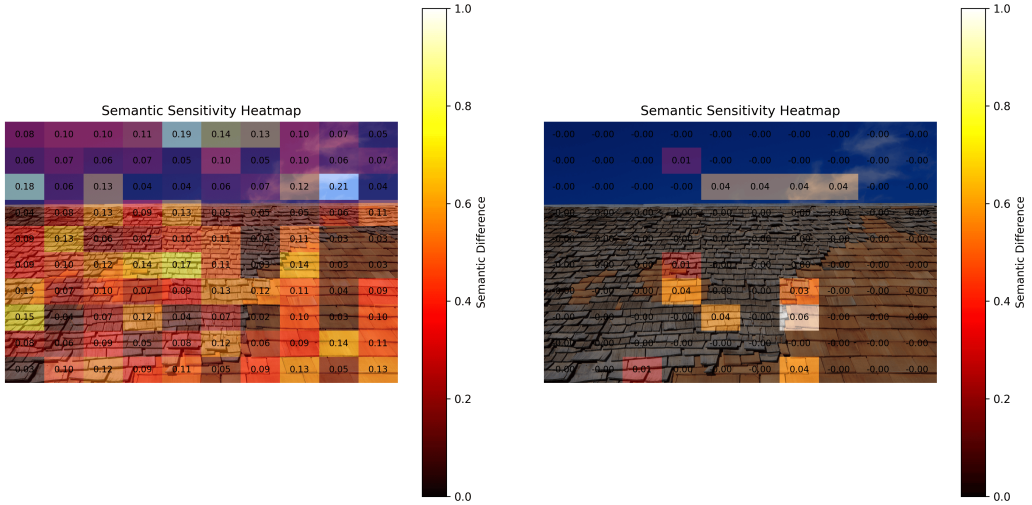

(a) GPT Heatmap (b) LLaVA Heatmap

Figure B.10: Forward Occlusion—Damaged Roof 1

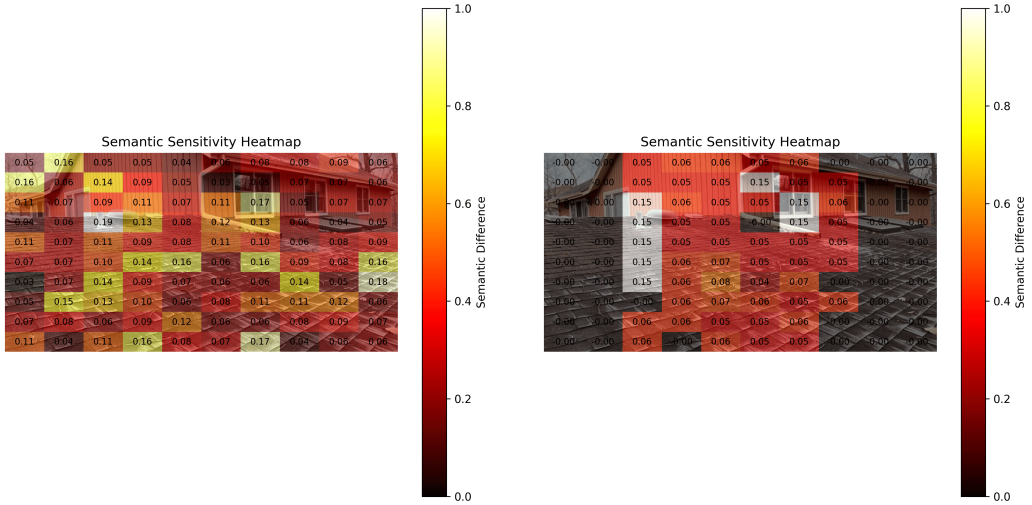

(a) GPT Heatmap (b) LLaVA Heatmap

Figure B.11: Forward Occlusion—Damaged Roof 2

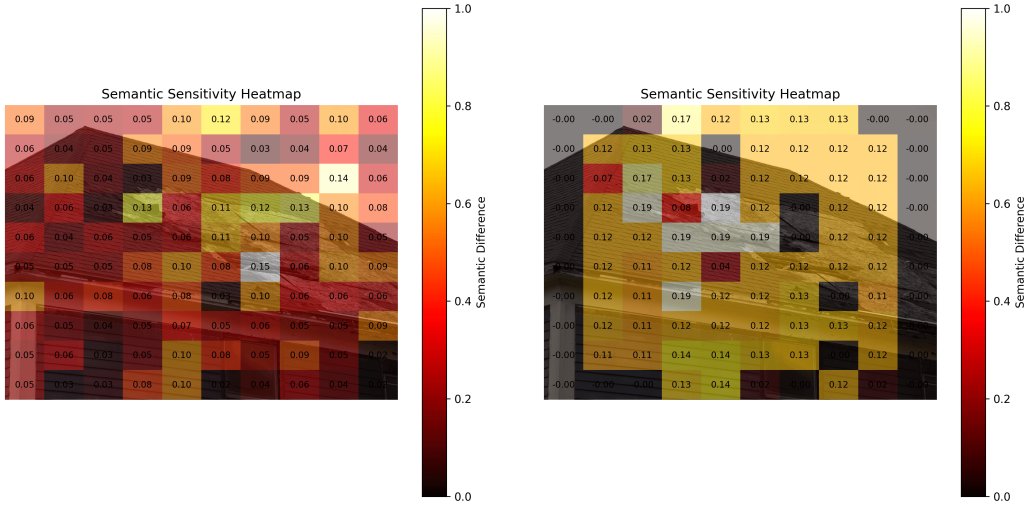

(a) GPT Heatmap (b) LLaVA Heatmap

Figure B.12: Forward Occlusion—Damaged Roof 3

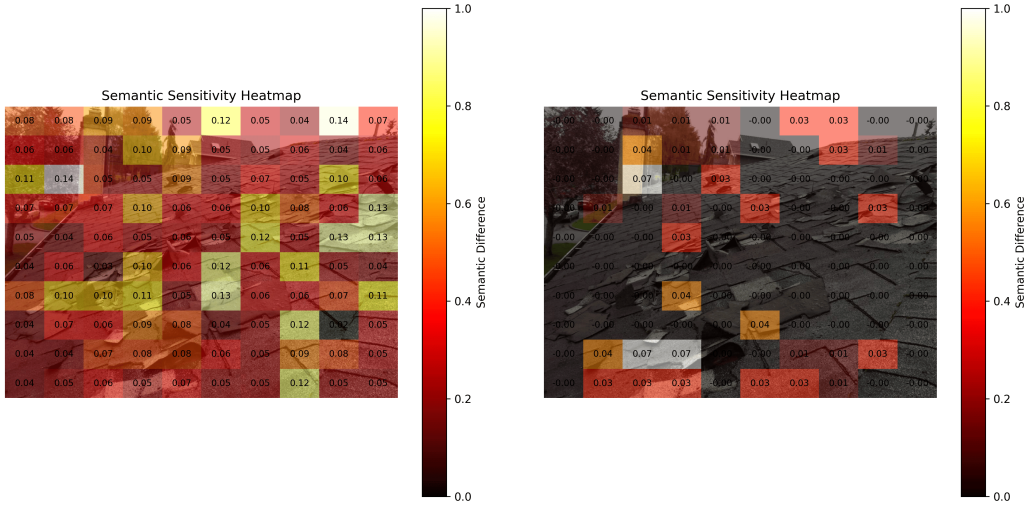

(a) GPT Heatmap (b) LLaVA Heatmap

Figure B.13: Forward Occlusion—Damaged Roof 4

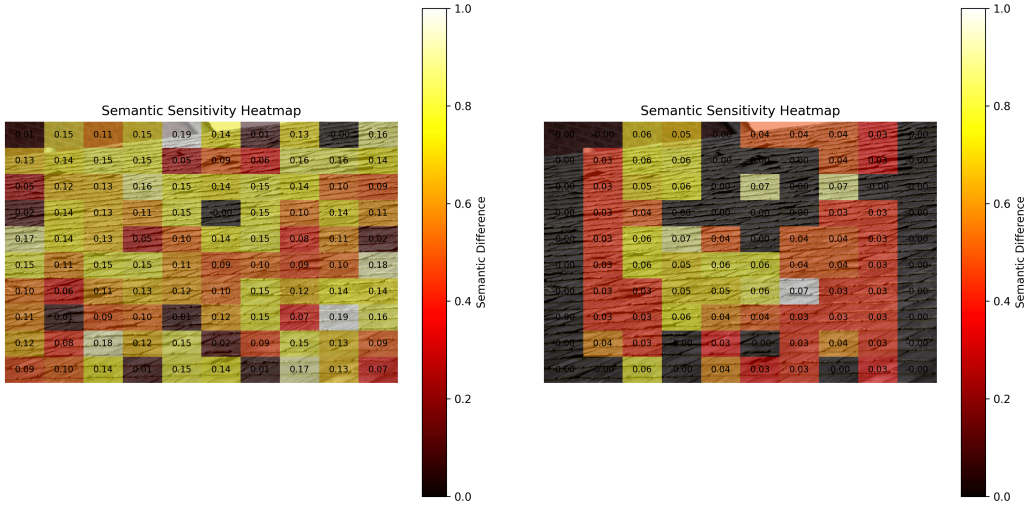

(a) GPT Heatmap (b) LLaVA Heatmap

Figure B.14: Forward Occlusion—Damaged Roof 5

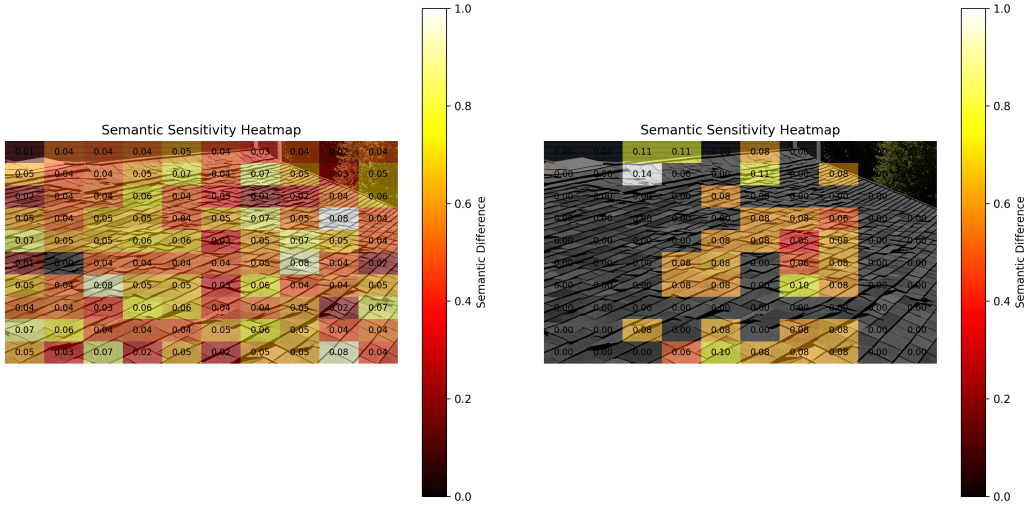

(a) GPT Heatmap (b) LLaVA Heatmap

Figure B.15: Forward Occlusion—Damaged Roof 6

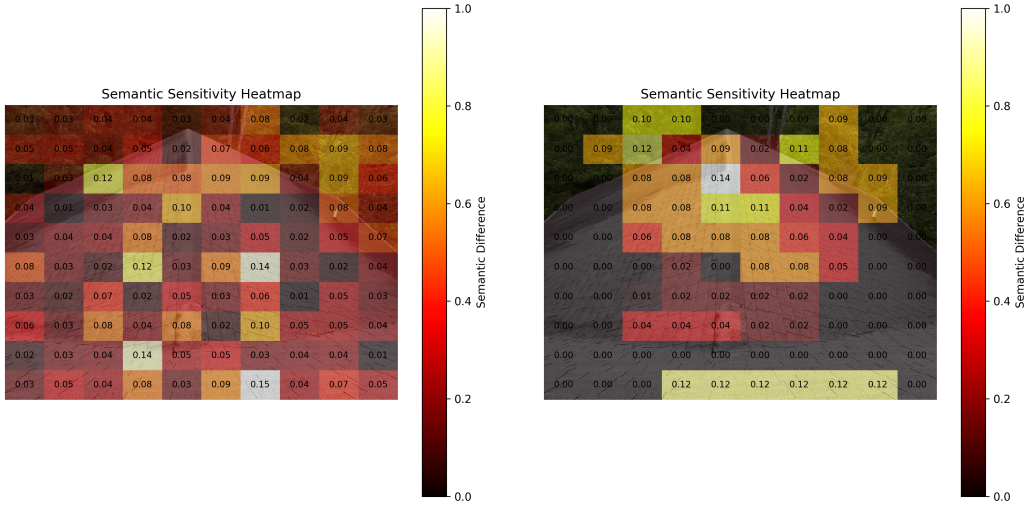

(a) GPT Heatmap (b) LLaVA Heatmap

Figure B.16: Forward Occlusion—Damaged Roof 7

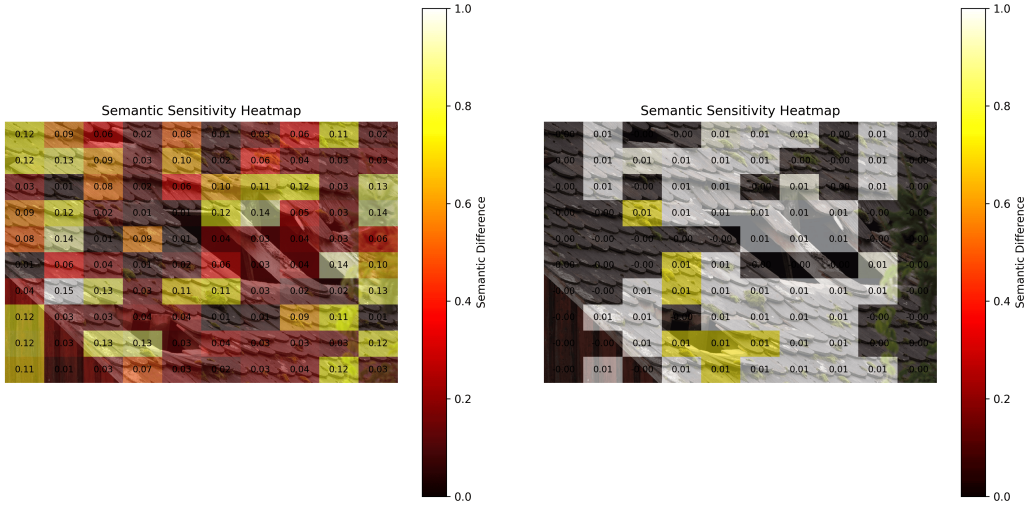

(a) GPT Heatmap (b) LLaVA Heatmap

Figure B.17: Forward Occlusion—Damaged Roof 8

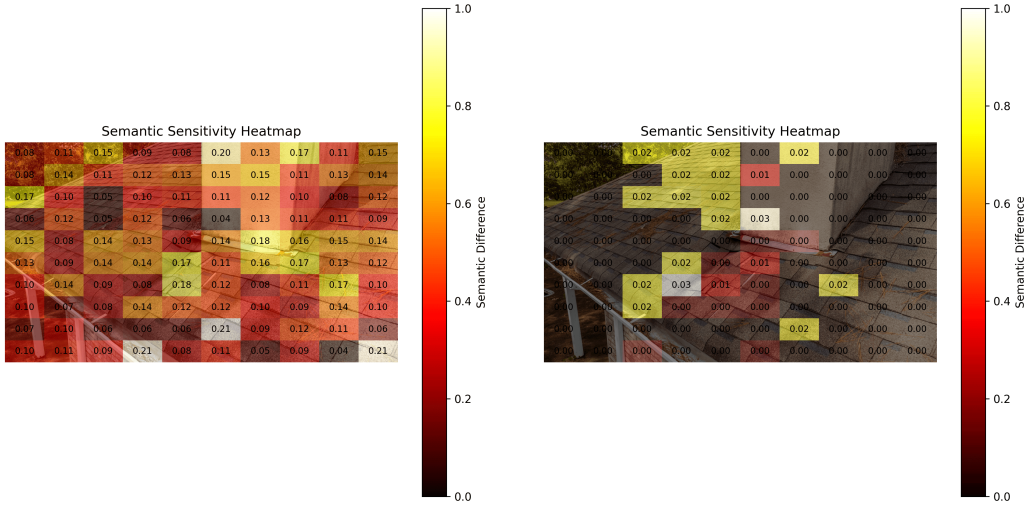

(a) GPT Heatmap (b) LLaVA Heatmap

Figure B.18: Forward Occlusion—Damaged Roof 9

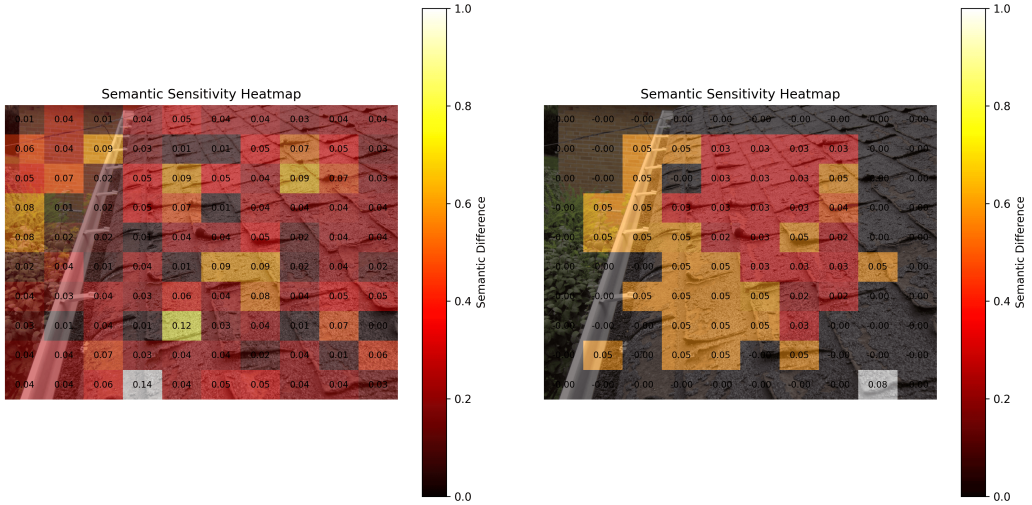

(a) GPT Heatmap (b) LLaVA Heatmap

Figure B.19: Forward Occlusion—Damaged Roof 10

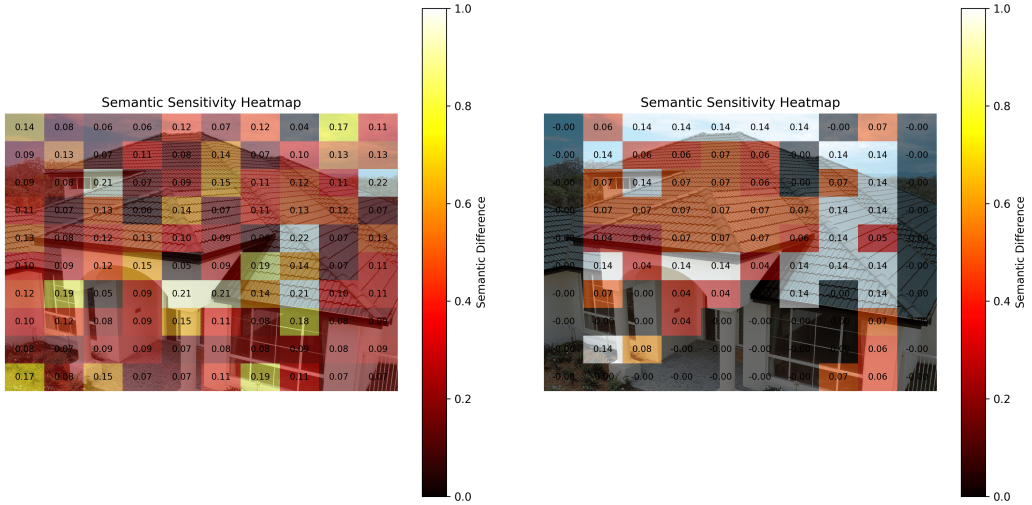

(a) GPT Heatmap (b) LLaVA Heatmap

Figure B.20: Forward Occlusion—Undamaged Roof 1

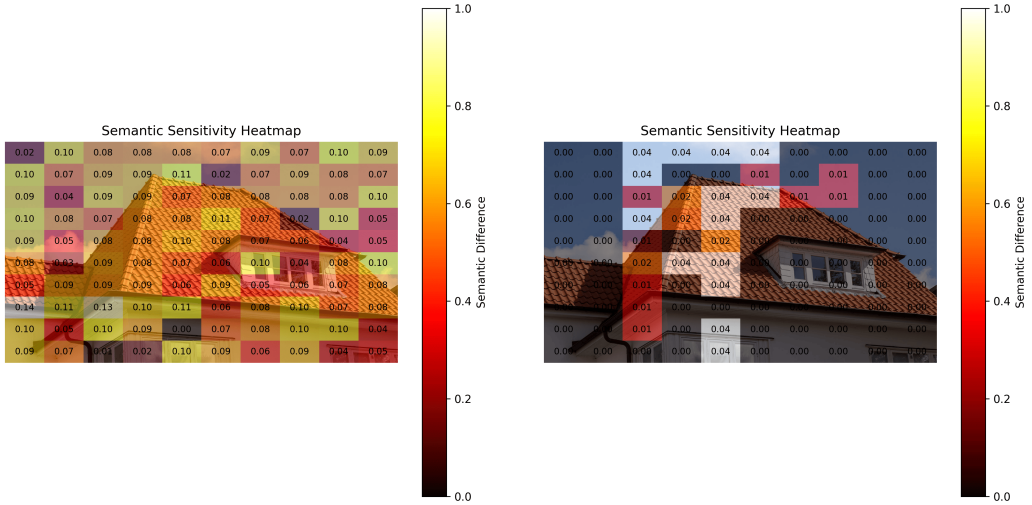

(a) GPT Heatmap (b) LLaVA Heatmap

Figure B.21: Forward Occlusion—Undamaged Roof 2

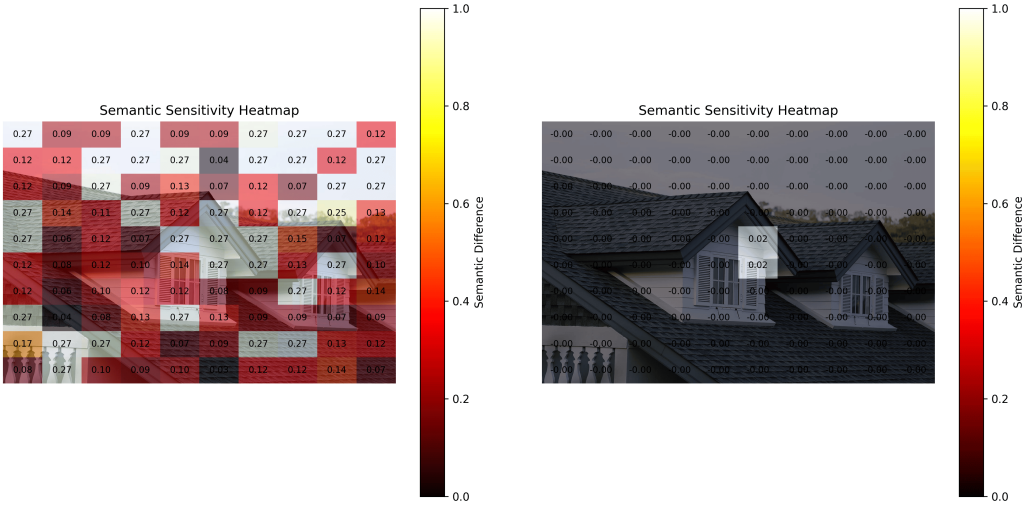

(a) GPT Heatmap (b) LLaVA Heatmap

Figure B.22: Forward Occlusion—Undamaged Roof 3

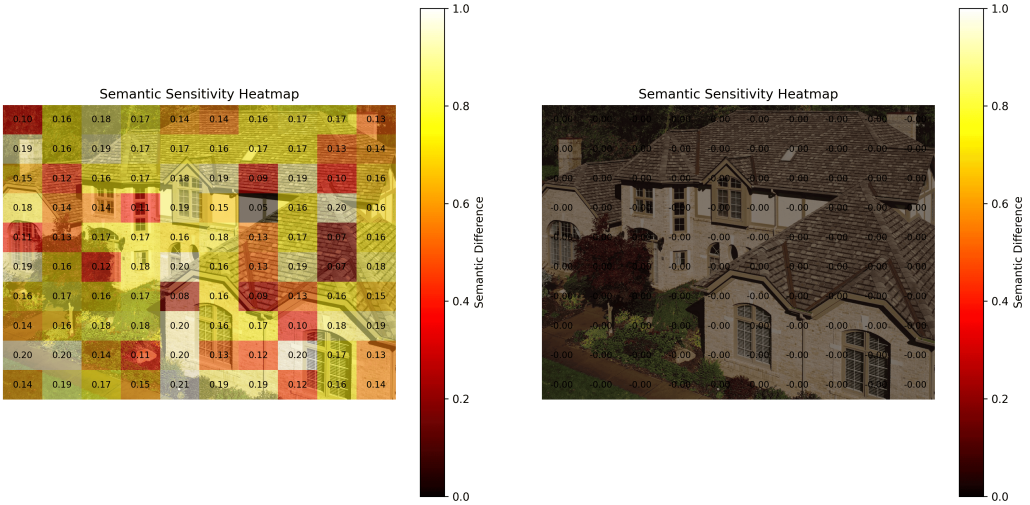

(a) GPT Heatmap (b) LLaVA Heatmap

Figure B.23: Forward Occlusion—Undamaged Roof 4

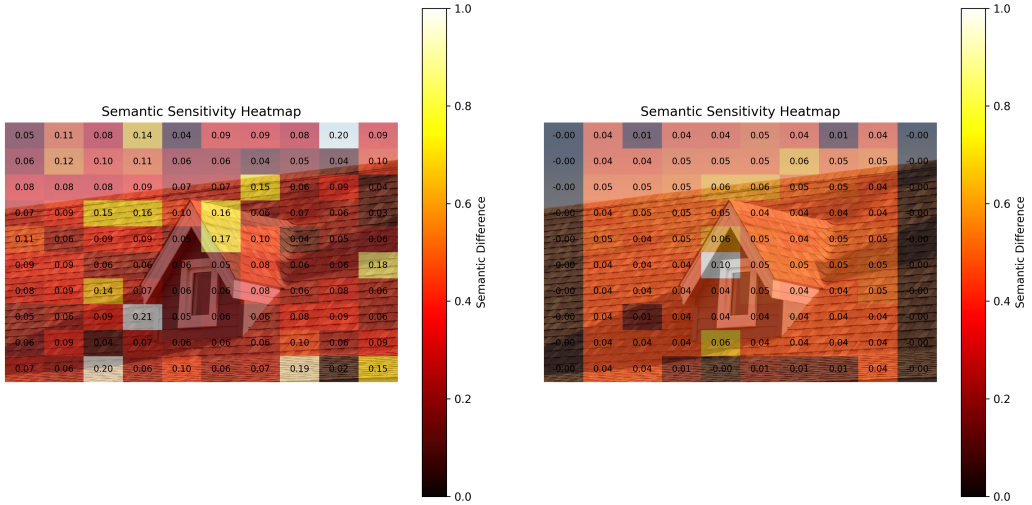

(a) GPT Heatmap (b) LLaVA Heatmap

Figure B.24: Forward Occlusion—Undamaged Roof 5

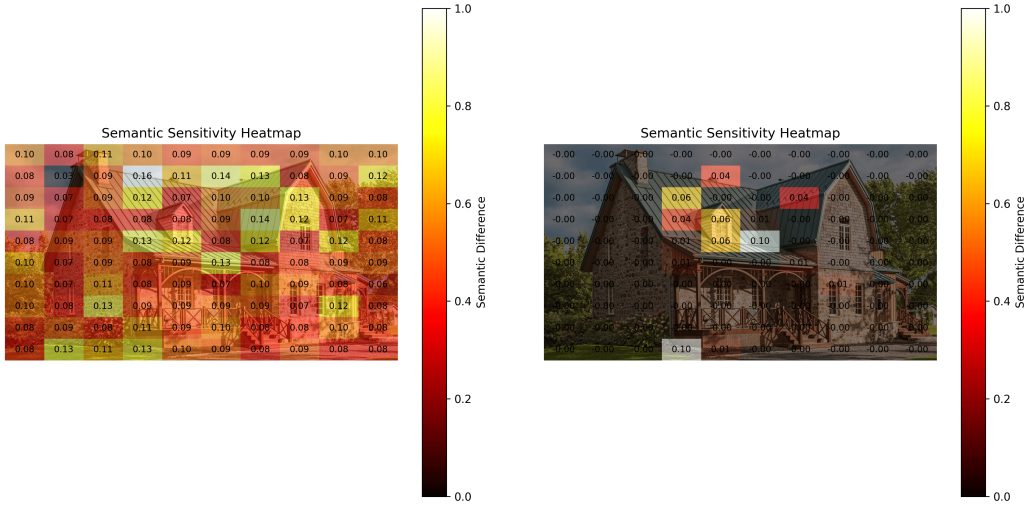

(a) GPT Heatmap (b) LLaVA Heatmap

Figure B.25: Forward Occlusion—Undamaged Roof 6

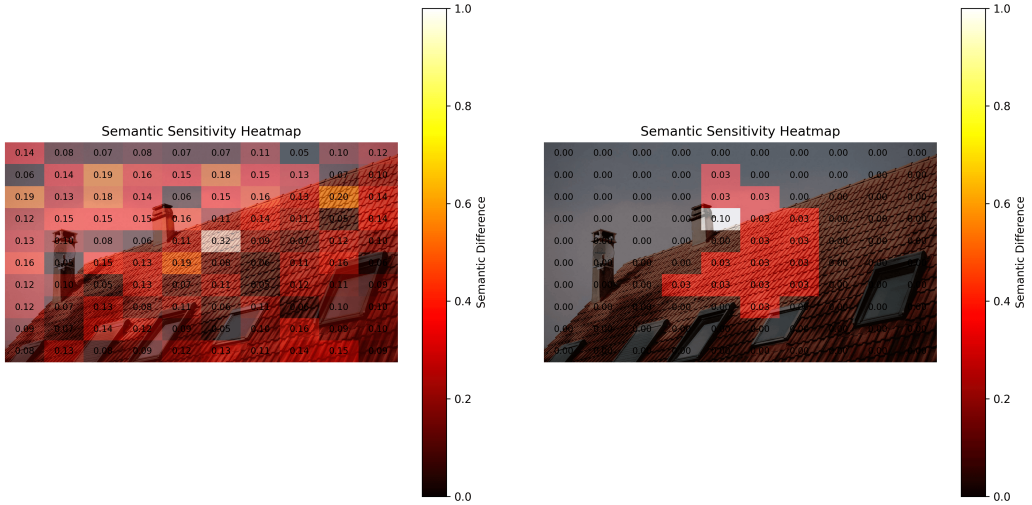

(a) GPT Heatmap (b) LLaVA Heatmap

Figure B.26: Forward Occlusion—Undamaged Roof 7

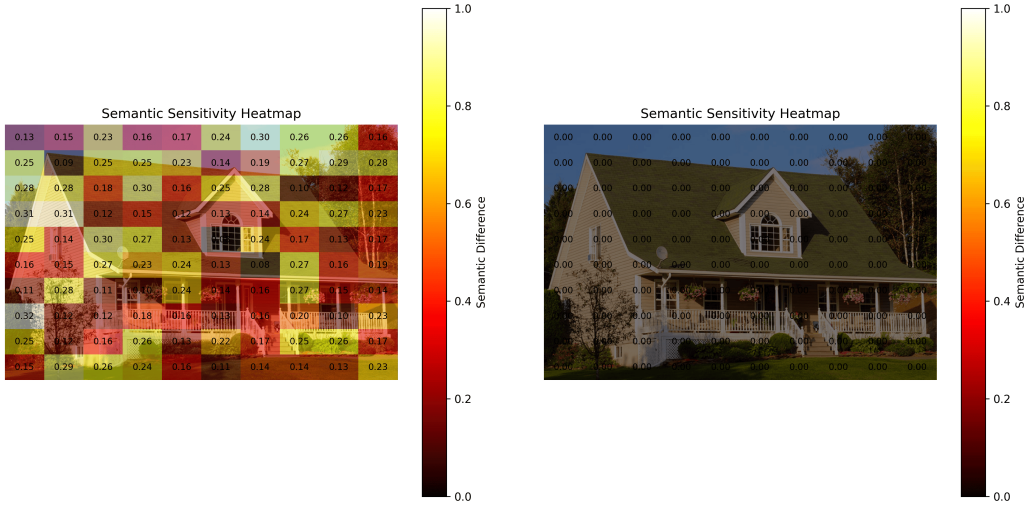

(a) GPT Heatmap (b) LLaVA Heatmap

Figure B.27: Forward Occlusion—Undamaged Roof 8

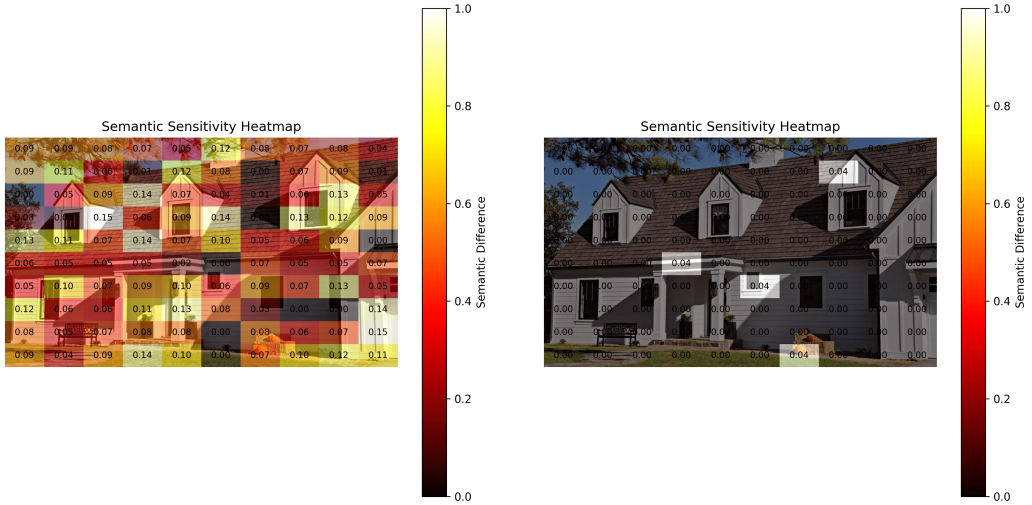

(a) GPT Heatmap (b) LLaVA Heatmap

Figure B.28: Forward Occlusion—Undamaged Roof 9

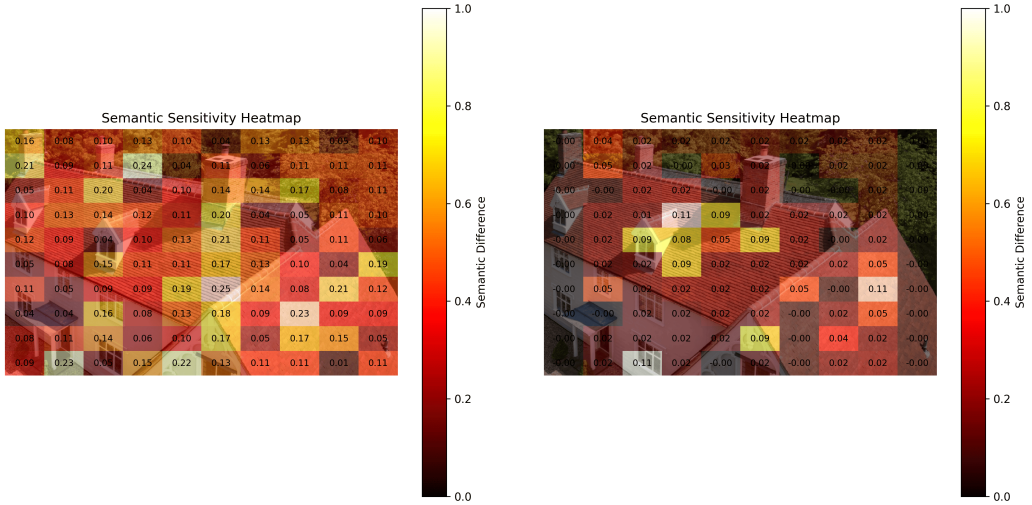

(a) GPT Heatmap (b) LLaVA Heatmap

Figure B.29: Forward Occlusion—Undamaged Roof 10